RESEARCH ARTICLE

NANO · MICRO small
www.small-journal.com

Highly Selective and Reversible Detection of Simulated Breath Hydrogen Sulfide Using Fe-Doped CuO Hollow Spheres: Enhanced Surface Redox Reaction by Multi-Valent Catalysts

Ki Beom Kim, Myung Sung Sohn, Sunhong Min, Ji-Wook Yoon, Jin-Sung Park, Ju Li, Young Kook Moon, and Yun Chan Kang**

The precise and reversible detection of hydrogen sulfide (H_2S) at high humidity condition, a malodorous and harmful volatile sulfur compound, is essential for the self-assessment of oral diseases, halitosis, and asthma. However, the selective and reversible detection of trace concentrations of H_2S (≈0.1 ppm) in high humidity conditions (exhaled breath) is challenging because of irreversible H_2S adsorption/desorption at the surface of chemiresistors. The study reports the synthesis of Fe-doped CuO hollow spheres as H_2S gas-sensing materials via spray pyrolysis. 4 at.% of Fe-doped CuO hollow spheres exhibit high selectivity (response ratio ≥ 34.4) over interference gas (ethanol, 1 ppm) and reversible sensing characteristics (100% recovery) to 0.1 ppm of H_2S under high humidity (relative humidity 80%) at 175 °C. The effect of multi-valent transition metal ion doping into CuO on sensor reversibility is confirmed through the enhancement of recovery kinetics by doping 4 at.% of Ti- or Nb ions into CuO sensors. Mechanistic details of these excellent H_2S sensing characteristics are also investigated by analyzing the redox reactions and the catalytic activity change of the Fe-doped CuO sensing materials. The selective and reversible detection of H_2S using the Fe-doped CuO sensor suggested in this work opens a new possibility for halitosis self-monitoring.

1. Introduction

The increasing interest in human health has led to increasing attention being given to diagnostic tests. Various methods for disease diagnosis, such as blood tests, have long been employed. However, these methods are invasive (causing user discomfort), and sometimes time-consuming, and require an expert analyst. In contrast, the diagnosis of specific diseases via the detection of human breath is non-invasive, fast, and usable by the general public, which has led to many studies in recent years.[1–5]

Hydrogen sulfide (H_2S) is a biomarker gas released into the exhaled breath of patients with oral diseases or halitosis.[6,7] Patients need to monitor H_2S concentration from their exhaled breath since others can feel uncomfortable while talking if a certain amount of H_2S is exhaled from the patient's breath and the presence of halitosis can be an indicator of overlooked serious inflammation in body. Additionally, to date, lots of investigation reported that exhaled H_2S provide more description of asthma phenotypes and possibly leads to improvements in the diagnosis and treatment of asthmatic patient.[8–10] Lastly, the exhaled breath can be related to intestinal diseases.[11] However, checking one's own smell is difficult because the human nose is easily fatigued. Therefore, the precise detection of H_2S in human exhaled breath can provide new possibilities for simple disease diagnosis based on breath analysis.

K. B. Kim, M. S. Sohn, S. Min, J.-S. Park, Y. C. Kang
Department of Materials Science and Engineering
Korea University
Seoul 02841, Republic of Korea
E-mail: yckang@korea.ac.kr

J.-W. Yoon
Department of Information Materials Engineering
Division of Advanced Materials Engineering
Jeonbuk National University
Jeonju 54896, Republic of Korea

The ORCID identification number(s) for the author(s) of this article can be found under https://doi.org/10.1002/smll.202308963

DOI: 10.1002/smll.202308963

J.-S. Park, J. Li
Department of Nuclear Science and Engineering
Massachusetts Institute of Technology
Cambridge, MA 02139, USA

J. Li
Department of Materials Science and Engineering
Massachusetts Institute of Technology
Cambridge, MA 02139, USA

Y. K. Moon
Department of Functional Ceramics
Ceramic Materials Division
Korea Institute of Materials Science (KIMS)
Changwon 51508, Republic of Korea
E-mail: ykmoon@kims.re.kr

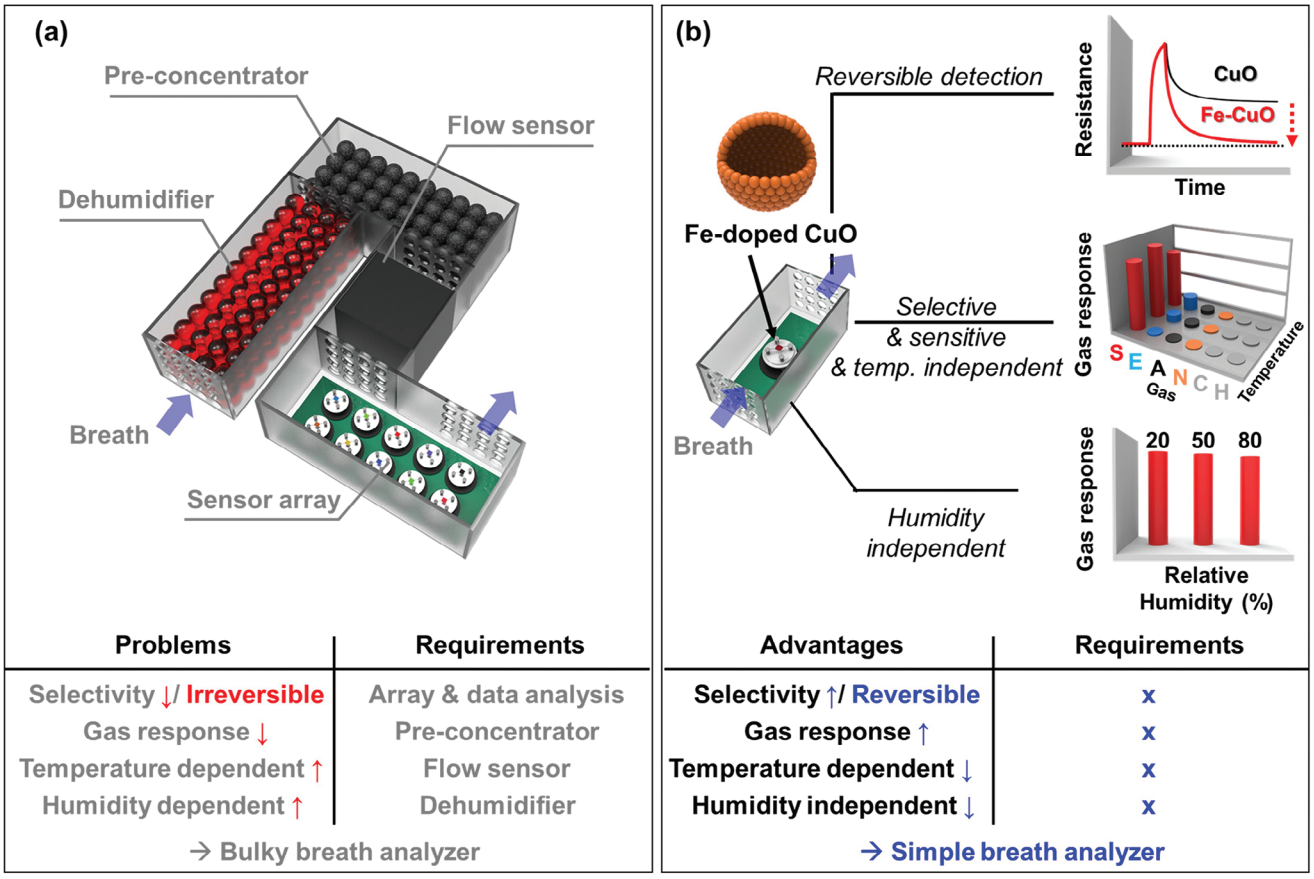

Scheme 1. a) Peripheral components for a breath analyzer via insufficient performance gas sensors. b) A novel gas sensing material with a Fe-doped CuO sensor is suggested as a solution for the selectivity, sensitivity, reversibility, and reliable detection of analyte gas toward oxide chemiresistors for a simple-structured breath analyzer (S: hydrogen sulfide, E: ethanol, A: acetone, N: ammonia, C: carbon monoxide, and H: hydrogen).

Conventional equipment for accurately detecting gas concentrations includes gas chromatography-mass spectrometry and proton transfer reaction-mass spectrometry. However, the necessary apparatus is too large and heavy and require operation by skilled operators. In contrast, metal oxide semiconductor (MOS) gas sensors can be mounted in a portable device because they are cheap, small-scale, and can detect target gases by simple resistance changes of the sensing materials.[12–18] However, the concentration of H_2S gas in exhaled breath is too low (≈0.1 ppm)[7] for reliable detection, and various interfering gases (H_2, ethanol, acetone, etc.) that inhibit accurate H_2S detection are present in human breath. Moreover, because the sensing characteristics of metal-oxide gas sensors are significantly degraded by humidity, it is extremely difficult to detect H_2S in exhaled human breath in a highly sensitive and selective manner, which require the peripheral components such as dehumidifier, preconcentrator, flow sensor, and sensor array hindering the miniaturization of breath analyzer (**Scheme** 1a). Therefore, highly selective and sensitive sensing materials that can operate at high humidity must be investigated to achieve accurate H_2S detection.

Copper oxide (CuO) is considered a superior sensing material for the sensitive and selective detection of H_2S gases. As CuO has a high chemical affinity for H_2S, it can not only detect H_2S at the sub-ppm level in a sensitive manner but also has high selectivity among other interference-exhaled breath biomarker gases (H_2, ethanol, acetone, etc.) at a relatively low temperature.[19–21] For instance, Chen et al.[22] reported selective H_2S gas sensors using CuO nanowire arrays, and Zhang et al.[20] reported selective H_2S gas sensors using CuO nanosheets. However, the reversibility of the above-mentioned sensing materials to H_2S is too low to be used in real applications. This is because of the sluggish kinetics of H_2S desorption due to the strong interaction between CuO and H_2S or the low reoxidation rate of $CuSO_4$ formed by the adsorption reaction.[23–25] Thus, enhancing the reversibility of CuO-based H_2S gas sensors, which is very important for breath analysis, remains a challenging issue and requires a breakthrough.

Herein, we report highly sensitive, selective, and reversible H_2S sensors using Fe-doped CuO hollow spheres prepared via spray pyrolysis. The sensor exhibited high sensitivity and exclusive selectivity toward H_2S over other biomarker gases under high humidity conditions (relative humidity: 80%) via high chemical affinity between CuO and H_2S. Furthermore, doping Fe ions into CuO has been suggested to achieve complete and rapid recovery, assisted by the facile redox reaction between the Fe^{3+}/Fe^{2+} pair.[26] The effects of the enhanced redox reaction on sensor reversibility were confirmed by Temperature-Programmed

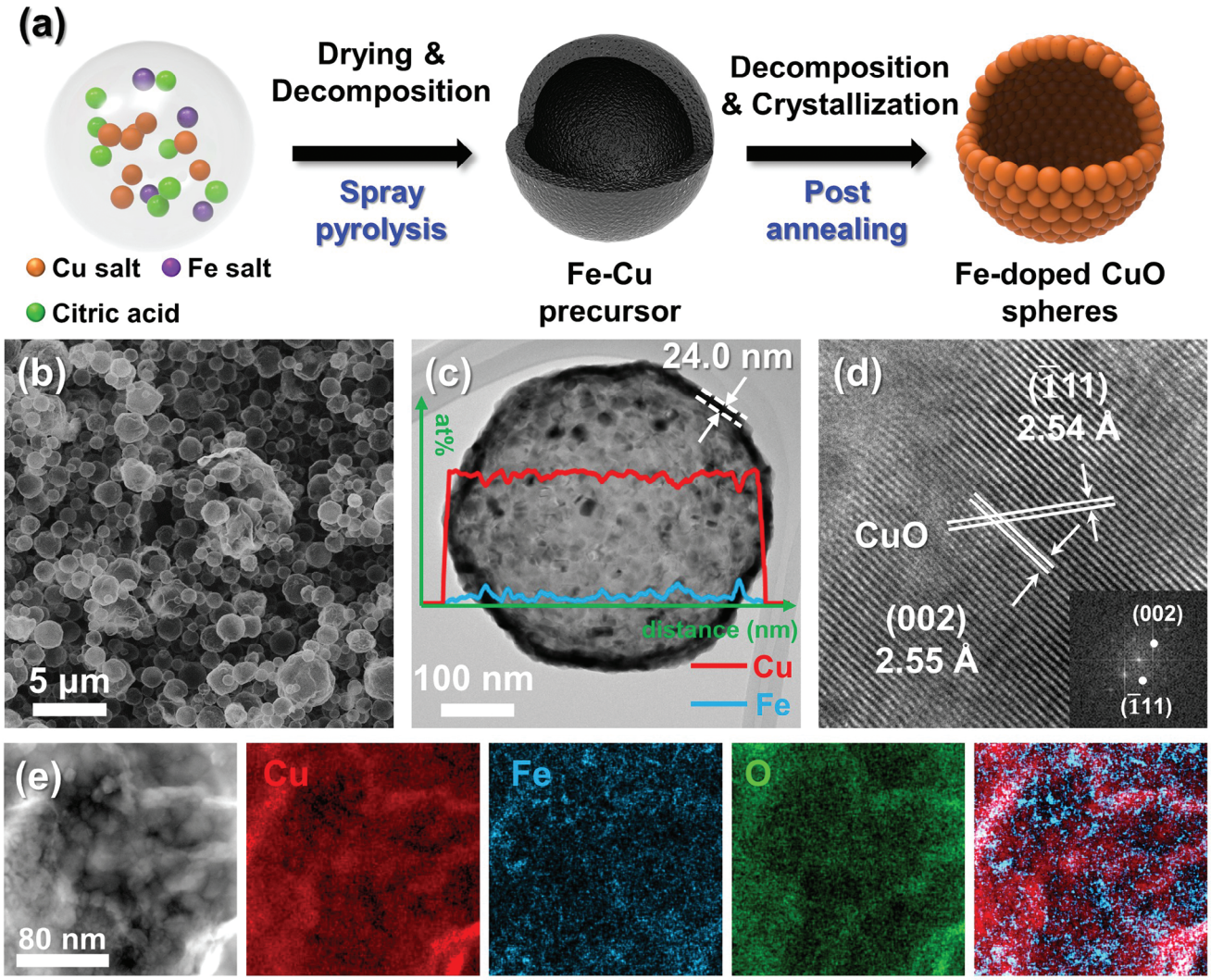

Figure 1. a) Scheme for the formation mechanism of Fe-doped CuO hollow spheres; b) SEM, c) TEM images and EDS line scan, d) HR-TEM lattice fringes, and e) elemental mapping images of 4Fe-CuO hollow spheres.

Reduction by Hydrogen (H_2-TPR). Additionally, the Fe-doped CuO sensor demonstrated superior gas sensing characteristics over a wide range of humidity (R.H.: 20–80%) and temperatures (175–225 °C), enabling the minimization of additional components for a breath analyzer (Scheme 1b). Lastly, the doping of multi-valent Ti or Nb ions into CuO can also enhance the selectivity and gas recovery characteristics of CuO-based sensors to H_2S, confirming that the proposed method is a novel and general solution for enhancing sensor performance. Although additional clinical research should be conducted to implement real-time detection of breath H_2S through oxide gas sensors, the sensors proposed in this work provide new pathways for diagnosis halitosis. The main focus of this study was to understand the gas-sensing mechanism underlying the reversible and selective detection of exhaled hydrogen sulfide in relation to the facile redox reaction derived from multi-valent elements and the change in catalytic activity via additives on the surface of metal oxide gas sensors.

2. Results and Discussion

A schematic of the synthesis procedure for the Fe-doped CuO is shown in **Figure** 1a. First, droplets containing Cu, Fe nitrate, and citric acid monohydrate underwent drying and decomposition during spray pyrolysis, and the precursor powders were collected using a Teflon bag filter. Second, the precursor powders were completely decomposed and crystallized through heat-treated at 450 °C for 2 h in air. The morphologies of pure CuO, 2, 4, and 8 at.% Fe-doped CuO (referred as 2Fe-CuO, 4Fe-CuO, and 8Fe-CuO, respectively) are shown in Figure 1b,c, and Figure S1 (Supporting Information), respectively. The pure and Fe-doped CuO powders exhibited hollow and spherical morphologies with semi-transparent shells, regardless of composition. Their hollow structure was also confirmed by dark contours of TEM images, which showed that they had a mean shell thickness of 24 ± 6 nm. In the lattice fringe of HR-TEM image and fast Fourier transform electron diffraction pattern for 4Fe-CuO, lattice planes with 2.55 and

2.54 Å, which corresponded to the (002) and ($\bar{1}$11) fringes of monoclinic CuO phase (JCPDS# 48–1548), were observed (Figure 1d). Additionally, the distributions of Cu, Fe, and O ions in 4Fe-CuO were confirmed by TEM-EDS mapping (Figure 1e). Although there was a slight agglomeration, the Fe ions were uniformly distributed along with the Cu ions. The relatively uniform distribution of Cu and Fe ions was also confirmed by EDS line scan image of 4Fe-CuO spheres (Figure 1c). The lattice planes of monoclinic CuO phase were also observed in pure, 2Fe-, and 8Fe-CuO spheres (Figure S1a$_3$–c$_3$, Supporting Information) and the lattice planes with 2.96 Å, which corresponded to the (112) and ($\bar{1}\bar{1}$2) fringes of cubic $CuFe_2O_4$ phase (JCPDS# 77-0010), were observed in 8Fe-CuO spheres (Figure S1c$_4$, Supporting Information). The particle size distributions of all specimens were analyzed by measuring the diameters of 300 spheres from the SEM images (Figure S2, Supporting Information). The average diameters of pure, 2Fe-, 4Fe-, and 8Fe-CuO hollow spheres were 0.73 ± 0.31, 0.83 ± 0.44, 0.76 ± 0.34, and 0.69 ± 0.28 µm, respectively, indicating the addition of Fe ions into CuO did not affect the size of the sensing materials.

The crystal structures of the pure, 2Fe-, 4Fe-, and 8Fe-CuO hollow spheres were investigated using X-ray diffraction (XRD) analysis (**Figure** 2a$_1$–d$_1$). They show only the monoclinic CuO phase (JCPDS # 48–1548), and no secondary phase peaks are observed (e.g., Fe_2O_3, Fe_3O_4, $CuFe_2O_4$). This can be attributed to the doping of Fe ions into the CuO lattice or to the detection limits of the XRD analysis. The average CuO crystallite sizes of pure, 2Fe-, 4Fe-, and 8Fe-CuO spheres were calculated to be 25.1 ± 2, 15.7 ± 0.7, 16.5 ± 1.9, and 16.9 ± 1.1 nm, respectively, using Scherrer's equation.

To further investigate the phase of the Fe-CuO spheres, all specimens were analyzed by Raman spectroscopy (Figure 2a$_2$–d$_2$). The peaks of pure CuO hollow spheres at ≈300 and ≈350 cm^{-1} correspond well with the literature data of pure CuO.[27–29] The 2Fe-, 4Fe-, and 8Fe-CuO hollow spheres exhibited similar Raman spectra to those of the pure CuO spheres. Note that no Fe-related peaks were observed in 2Fe- and 4Fe-CuO spheres, and only 8Fe-CuO showed a $CuFe_2O_4$ peak at ≈700 cm^{-1} (Figure 2a$_2$–d$_2$).[27,30] Considering the HR-TEM, EDS mapping images, XRD, and Raman analysis results of the Fe-doped CuO spheres, the Fe ions could be doped into the CuO lattice. In addition, a small amount of $CuFe_2O_4$ was present in the 4Fe-CuO spheres (Figure 1e), and a relatively large amount of $CuFe_2O_4$ was present in the 8Fe-CuO spheres (Figure 2d$_2$; Figures S1c$_4$, and S3, Supporting Information). In 8Fe-CuO, the possibility of the formation of other Fe-related phases (Fe_2O_3 and Fe_3O_4) was excluded because Cu ions also existed in the Fe-concentrated spots in the TEM elemental mapping images (Figure S3, Supporting Information). It should be noted that the ionic radius of Fe^{3+} (0.49 Å, coordination number = 4) is similar to the ionic radius of Cu^{2+} (0.57 Å, coordination number = 4), suggesting that some amount of Fe doping into the CuO lattice is feasible.[31–33] The formation of a secondary phase ($CuFe_2O_4$) in the 4Fe- and 8Fe-CuO spheres can be attributed to the large number of Fe ions, higher than the solubility (4–6 at.%), in the CuO matrix.[34,35]

The pore size distributions and specific surface areas (SSAs) of the pure and Fe-doped CuO hollow spheres were measured by Brunauer–Emmett–Teller (BET) analysis (Figure S4, Supporting Information). The SSAs of the pure, 2Fe-, 4Fe-, and 8Fe-CuO were 7.13, 10.52, 11.57, and 10.67 m^2g^{-1}, respectively. The increase in the SSAs due to Fe doping can be explained by the decrease in the crystallite size of CuO, which was confirmed by XRD analysis. In addition, the number of mesopores (2–50 nm), which have the advantage of gas accessibility, increased with the addition of Fe. These results suggest that the hollow structure of the sensing material is advantageous for facile gas accessibility.

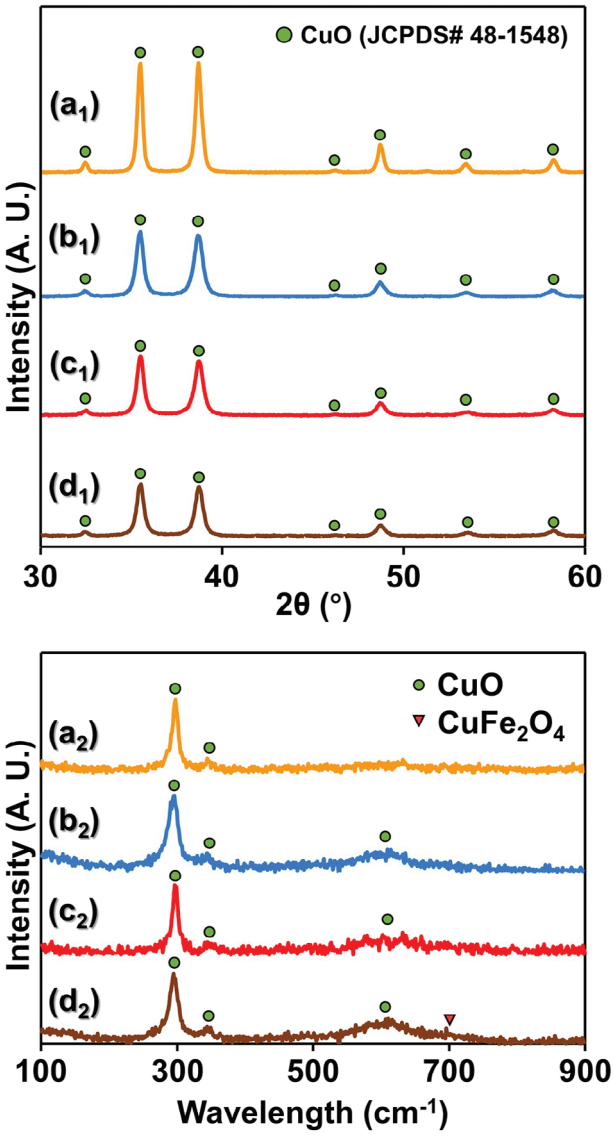

Figure 2. X-ray diffraction patterns and Raman spectroscopy of a$_1$,a$_2$) pure, b$_1$,b$_2$) 2Fe-, c$_1$,c$_2$) 4Fe-, and d$_1$,d$_2$) 8Fe-CuO hollow spheres.

The gas-sensing characteristics of the sensors to 0.1 ppm H_2S, 0.5 ppm acetone, 1 ppm ethanol, 5 ppm CO, NH_3, and 20 ppm H_2 were measured at 175–250 °C with RH 80% and the percent of resistance recovery to 0.1 ppm H_2S were also calculated overall the operating temperature (**Figure** 3). Because human breath contains a low concentration of H_2S and a relatively high

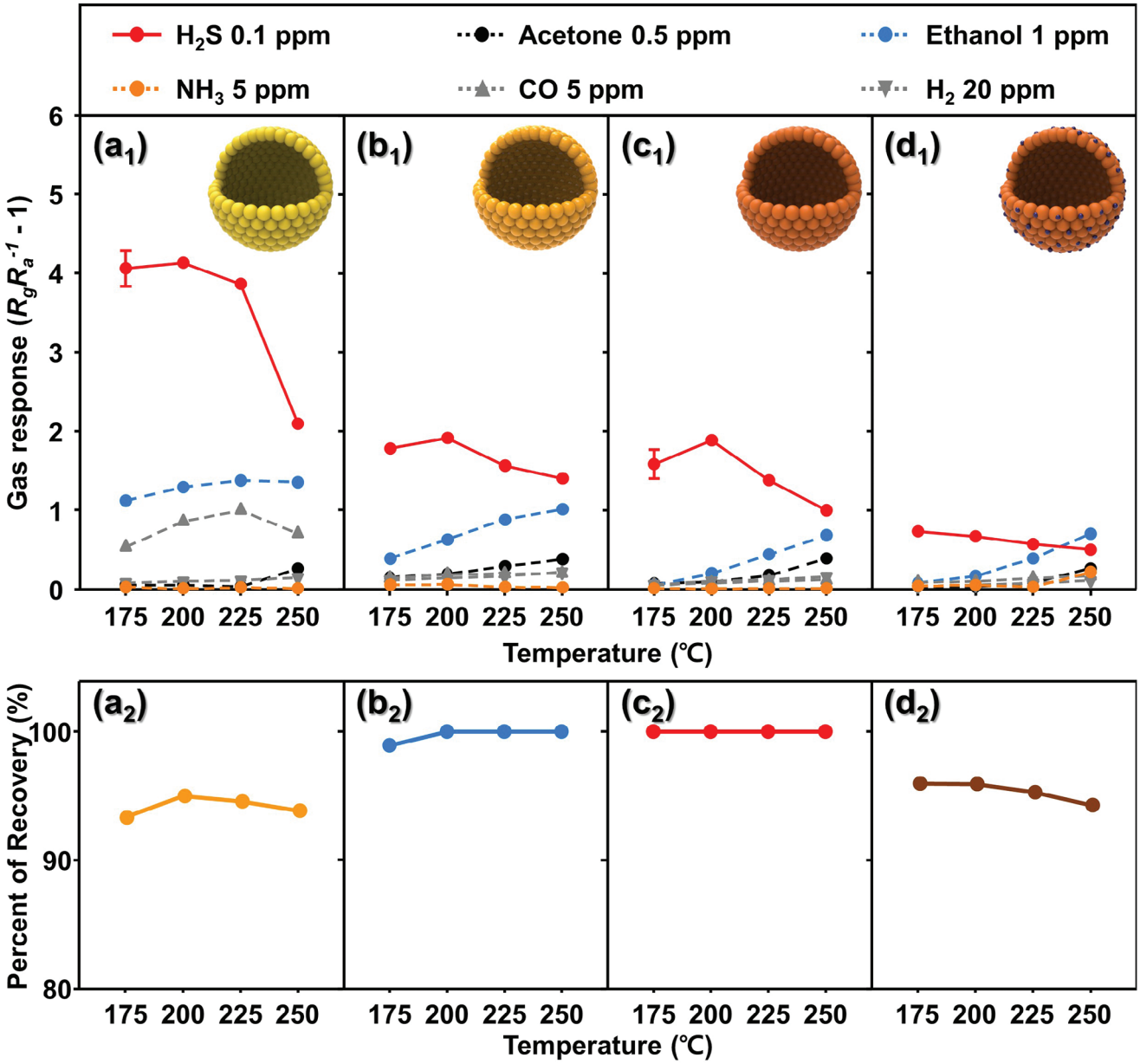

Figure 3. Gas response of a_1) pure, b_1) 2Fe-, c_1) 4Fe-, and d_1) 8Fe-CuO hollow spheres to 0.1 ppm H_2S, 0.5 ppm Acetone, 1 ppm Ethanol, 5 ppm NH_3, CO, and 20 ppm H_2 at 175–250 °C with RH 80%, and the percent of recovery values of a_2) pure, b_2) 2Fe-, c_2) 4Fe-, and d_2) 8Fe-CuO to 0.1 ppm H_2S at 175–250 °C.

concentration of other interfering volatile organic compounds that are generated by body metabolic or pathological processes, the measured concentrations of the H_2S (H_2S: 0.1 ppm) and interference gases were set based on the diagnostic reference or higher concentration (Acetone: 0.5 ppm, Ethanol: 1 ppm, CO: 5 ppm and H_2: 20 ppm) in the literature[36–39] at RH of 80%. All sensors exhibited the typical gas-sensing behavior of p-type oxide semiconductors; their resistance increased upon exposure to the reducing gas and returned to the initial value in an air atmosphere (Figure S5, Supporting Information). Therefore, the gas responses (S) of all the sensors are described by R_g/R_a–1 (R_g: resistance under the analyte gas, R_a: resistance in the humid air atmosphere). Furthermore, to investigate the reversibility of the gas sensors to H_2S, the percentage recovery (POR) was defined as $(R_{a,1}/R_{a,2}) \times 100$ ($R_{a,1}$: resistance before exposure to the analyte gas; $R_{a,2}$: resistance after exposure to the analyte gas).

The pure CuO sensor showed a higher gas response (S = 2.2–5.3) to 0.1 ppm of H_2S than other interfering gases, even under high humidity conditions (RH 80%) at all sensing temperatures. In contrast, the gas selectivity and the gas responses to H_2S gradually decreased as the gas-sensing temperatures increased (Figure 3a). Note that to improve the measurement accuracy, the gas-sensing characteristics toward analytic gases were measured in the order from interference gases to H_2S because the

baseline of the pure CuO sensor did not recover to the origin after exposure to H_2S gas. In general, CuO-based gas sensors exhibited high gas response and selectivity toward H_2S due to the high chemical affinity of CuO with H_2S or phase transformation of semiconducting CuO to metallic CuS ($CuO + H_2S_{(g)} \rightarrow CuS + H_2O_{(g)}$) at relatively high concentration of H_2S (resistance decreased after exposure to H_2S) or the H_2S oxidation with the pre-adsorbed oxygen ions $O^{\delta-}$ (e.g., O_2^-, O^-, O^{2-}) on the surface of CuO ($H_2S_{(g)} + 3O^{\delta-}_{(ads)} \rightarrow H_2O_{(g)} + SO_{2(g)} + 3e^-$) at relatively low concentrations of H_2S (resistance increased after exposure to H_2S).[40] Therefore, considering the resistance increase (Figure S5, Supporting Information) after exposure to H_2S, the high gas response to 0.1 ppm H_2S gas can be explained by the reaction with the pre-adsorbed oxygens on the surface of CuO.

However, the pure CuO hollow sphere sensor in this study not only failed to recover to the baseline resistance after being returned to an air atmosphere but also exhibited a relatively high response to interfering gases (e.g., ubiquitous ethanol), inhibiting the design of highly reversible and selective H_2S gas sensor at overall operating temperature (175–250 °C) (Figure $3a_1$–a_2). These results can be attributed to irreversible H_2S gas adsorption/desorption from the surface of the CuO hollow spheres.[40] In contrast, the reversibility of the gas-sensing characteristics increased significantly with the doping of Fe ions into CuO. Overall, the 2Fe-CuO sensor showed a higher percent of recovery (POR) than that of the pure CuO sensor, and the minimum reversible sensing temperature decreased to ≥ 200 °C (POR = 98.9% at 175 °C) (Figure $3b_2$). The increase of Fe concentration to 4 at.% further enhanced the gas reversibility of the gas-sensing characteristics, and interestingly, the POR increased to 100% at ≥ 175 °C (Figure $3c_2$). Moreover, the selectivity of the 4Fe-CuO sensor to H_2S over other interference gases at the minimum reversible temperature (175 °C) was higher than those of other sensors, suggesting the doping of Fe ions into CuO can also enhance the H_2S gas selectivity (Figure $3b_1$–d_1). Accordingly, considering both the gas selectivity and reversibility of the sensors, the optimal sensing materials and temperature were 4Fe-CuO and 175 °C, respectively (Figure S6, Supporting Information). A low operating temperature is advantageous for reducing the power consumption of the heater, preventing the degradation of the sensing materials, and facilitating microelectromechanical system (MEMS)-compatible sensor packaging, which is essential for portable sensor modules.

Under actual gas sensing conditions, exhaled breath H_2S coexist with different concentrations of large number of gases, which often hinders quantifying gas concentrations. To determine the reliable sensing under interferants, the sensor responses to 0.1 ppm of H_2S and the same in mixed gases were measured at 175 °C by varying the interfering gas type and concentration (i.e., 0.5–5 ppm of ethanol, acetone, hydrogen, or CO) (Figure S7, Supporting Information). The 4Fe-CuO sensor exhibited nearly identical H_2S gas responses, regardless of the interfering gas (i.e., H_2S responses showed average variations of 3.45%). This result confirms the exceptional selectivity of 4Fe-CuO sensor for H_2S in gas mixtures, indicating the validity of the sensor in actual breath analyzing condition. However, the 8Fe-CuO sensor exhibited a lower POR value, response, and selectivity for H_2S than 4Fe-CuO. Considering the significant amount of the $CuFe_2O_4$ phase in 8Fe-CuO (Figure $2d_2$; Figures $S1c_4$ and S3, Supporting Information), these results suggest that only an appropriate amount of Fe doping into CuO is effective for detecting trace-level concentrations of H_2S gas with high reversibility and selectivity at low sensing temperatures. The excess $CuFe_2O_4$ phase can deteriorate the gas-sensing properties of Fe-doped CuO sensors.

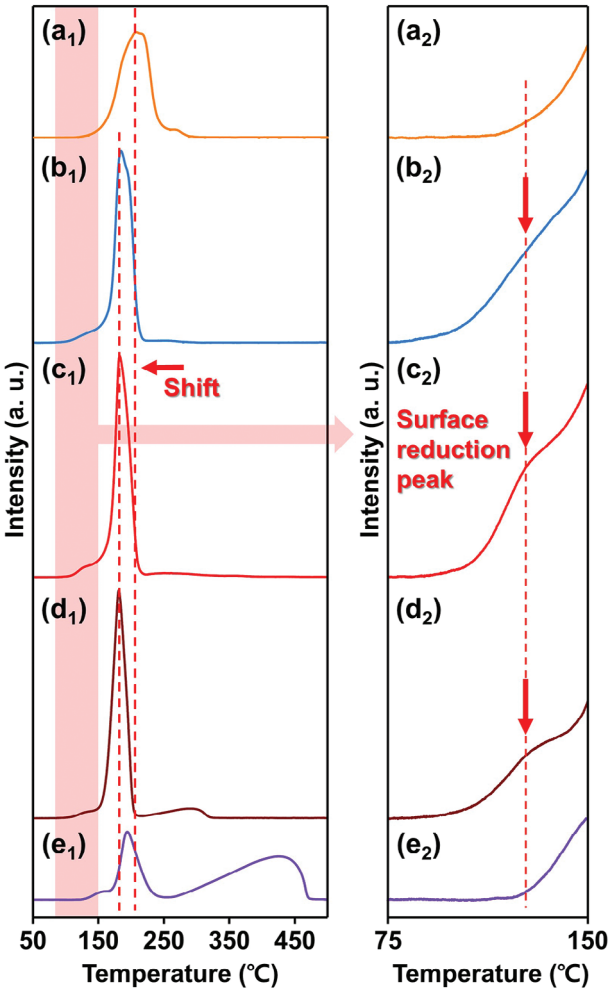

Figure 4. H_2-TPR analysis results of a_1,a_2) pure, b_1,b_2) 2Fe-, c_1,c_2) 4Fe-, d_1,d_2) 8Fe-CuO, and e) $CuFe_2O_4$ powders.

To understand the reversible gas-sensing characteristics, the contribution of Fe doping into CuO to enhanced reducibility was investigated using H_2-TPR analysis (**Figure 4**). The pure CuO exhibited major reduction peaks at ≈207 °C, indicating the reduction of bulk CuO. In contrast, as the Fe doping amount increased to 4 at.%, the Fe-doped CuO exhibited major reduction peaks at ≈180 °C and minor reduction peaks at ≈125 °C, indicating that the reduction ability of the sensing materials could be enhanced by doping Fe into the CuO.[41,42] Additionally, the $CuFe_2O_4$ exhibited a minor surface reduction peak at ≈150 °C, a major bulk reduction peak at ≈195 °C, and Fe component reduction peaks at 300–450 °C. Notably, the minor surface reduction peaks at low temperatures appearing in the H_2-TPR results for 2Fe- and 4Fe-CuO had the same tendency as the POR values. If the adsorbed oxygen is easily desorbed on the surface, oxygen can also be easily adsorbed on the surface again, inducing

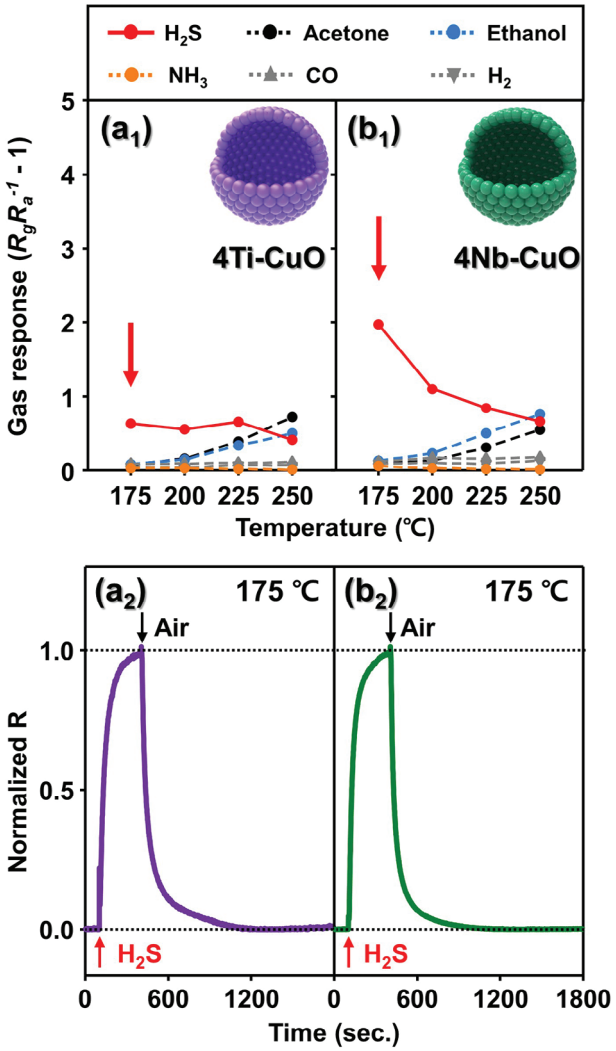

Figure 5. Gas response of a_1) 4Ti-, and b_1) 4Nb-CuO sensors to 0.1 ppm H_2S, 0.5 ppm Acetone, 1 ppm Ethanol, 5 ppm NH_3, CO, and 20 ppm H_2 at 175–250 °C with RH 80%, and the normalized sensing transients of a_2) 4Ti-, and b_2) 4Nb-CuO sensors to 0.1 ppm H_2S at 175 °C.

H_2S desorption from the surface and perfect resistance recovery of the CuO sensors. However, 8Fe-CuO did not exhibit perfect recovery to H_2S despite showing a surface reduction peak at ≈125 °C, which seems related to a large amount of $CuFe_2O_4$ phase content (Figure 2d_2; Figures S1c_4 and S3, Supporting Information). The $CuFe_2O_4$ powder prepared by spray pyrolysis and subsequent heat treatment (Figure S8, Supporting Information) showed a higher surface reduction temperature than Fe-doped CuO (Figure 4e).[43] This strongly suggests that $CuFe_2O_4$ interferes with the redox reactions of oxygen molecules and degrades the reversibility of Fe-doped CuO sensors at low temperatures. Additionally, the H_2-TPR analysis results can explain the change in the catalytic activity of the Fe-doped CuO hollow spheres. Previous studies have shown that sensing materials with lower reduction peak temperatures in H_2-TPR analysis exhibit higher catalytic activity.[44–46] Therefore, the Fe-doped CuO hollow spheres exhibited higher catalytic activity than pure CuO. The influence of the change in catalytic activity on the gas-sensing characteristics is discussed later.

To further investigate the effect of the $CuFe_2O_4$ phase on the gas-sensing properties, 20Fe-CuO hollow spheres were prepared using the same method. In the XRD analysis, 20Fe-CuO exhibited a monoclinic CuO phase and large $CuFe_2O_4$ phase peaks at ≈480 and ≈700 cm^{-1} in Raman analysis (Figure S9a,b, Supporting Information). Also, the lattice planes with 2.32 and 4.83 Å, which corresponded to the (111) fringe of monoclinic CuO and (101) fringe of cubic $CuFe_2O_4$ phase, were observed (Figure S9c, Supporting Information). The gas-sensing characteristics of 20Fe-CuO and the POR to 0.1 ppm H_2S were evaluated at 175–250 °C with RH 80% (Figure S9d,e, Supporting Information). The 20Fe-CuO sensor exhibited a similar tendency to 8Fe-CuO, which also contained a significant amount of $CuFe_2O_4$ and exhibited a low response, selectivity, and reversibility to H_2S. These results additionally support that not the formation of $CuFe_2O_4$ on CuO but doping of Fe ions into CuO lattice can enhance the sensitivity, selectivity, or reversibility of CuO sensors to H_2S.

The high selectivity of the 4Fe-CuO sensors needs to be discussed in relation to the catalytic activity change of CuO and the difference in the diffusion rate between H_2S and interfering gases (ethanol and acetone). In our sensor configuration, the two electrodes are located at the bottom of the sensing film. Therefore, the gas response was determined by the transport and oxidation of the analyte gas in the sensing film, followed by a sensing reaction between the adsorbed oxygen and the analyte gas in the lower sensing film region. After doping the CuO sensor with Fe, the overall gas response decreased during diffusion through the catalytic sensing film. In particular, for the interfering gases, the gas responses decreased to negligible levels, which enhanced the H_2S selectivity. Note that Fe ion, with abundant oxygen adsorption and facile redox reactions, is known to be excellent catalysts for the oxidation of volatile organic compounds (ethanol, acetone, etc.). For example, Guy et al.[47] reported that CuO/Fe_2O_3 catalysts are more active for ethanol oxidation than pure Fe_2O_3 or pure CuO catalysts. Hu et al.[48] also prepared Fe-loaded Linde type-A zeolites by impregnation and heat treatment and determined their high catalytic activities for the oxidation of vapor-phase acetone. However, when the Fe doping amount was increased to 8 at.%, the response to H_2S further decreased, indicating that the oxidation of H_2S to reduce the gas response was promoted more by the excessive amount of catalytic Fe ions. Therefore, the high selectivity for H_2S in the 4Fe-doped CuO sensor can be attributed to the excessive oxidation of interfering gases by the highly catalytic Fe-doped CuO.

The effect of relative humidity on the 4Fe-CuO sensor characteristics, which is important for practical breath analysis, was investigated by measuring the gas sensing characteristics under different humidity conditions (RH 20%, RH 50%, and RH 80%) (Figure S10, Supporting Information). It is worth noting that the gas response and selectivity values of the 4Fe-CuO sensor were similar regardless of humidity variation (Figure S10, Supporting Information), confirming humidity-independent gas sensing characteristics. These results demonstrate that the fabricated sensor can be used to detect sub-ppm-level H_2S under a varied-humidity atmosphere in a highly sensitive and selective manners (e.g., breath analysis). Also, the 90% response and 90% recovery times (τ_{res} and τ_{recov}), the times to reach 90% of

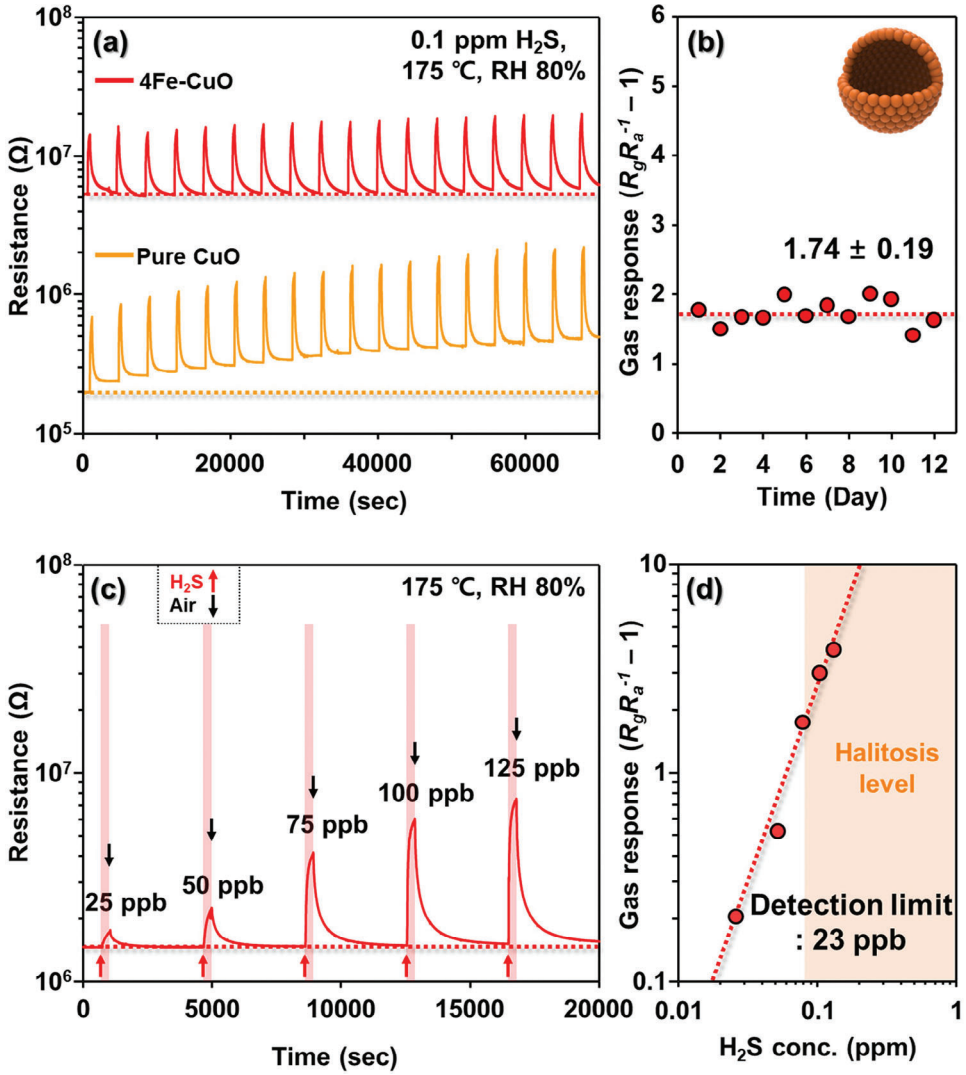

Figure 6. a) Eighteen-repetitive gas sensing transients of 4Fe-CuO and pure CuO to 0.1 ppm H_2S; b) long-term stability of 4Fe-CuO to 0.1 ppm H_2S; c) dynamic gas-sensing transients of 4Fe-CuO to 0.025–0.1 ppm H_2S; d) gas responses as a function of H_2S gas concentration (measurement temperature: 175 °C, relative humidity: RH80%).

resistance variation upon exposure to analyte gas and air, were calculated from the sensing transients at 175–250 °C (Figure S11, Supporting Information). The τ_{res} values ranged from 107 to 201 s and the τ_{recov} values ranged from 174 to 409 s. The τ_{res} and τ_{recov} values of 4Fe-CuO sensor was sufficient for practical breath analysis.

The most intriguing result of this work is the significant enhancement of gas recovery kinetics by introducing multi-valent metal ions into CuO. This enhancement can be explained by the facile redox reaction assisted by the multi-valent Fe ions in Fe-CuO. Because Fe is multi-valent, occurring as Fe^{3+}/Fe^{2+}, the re-adsorption, and ionization of oxygen can occur easily by the reduction of high valence cations to lower-valence states (e.g., from Fe^{3+} to Fe^{2+}). In fact, in the X-ray photoelectron spectra (XPS) data, Fe $2p_{3/2}$ and $2p_{1/2}$ peaks were observed at 710.5 and 723.2 eV in 4Fe-CuO and could be deconvoluted into Fe^{2+} and Fe^{3+} peaks (Figure S12, Supporting Information). These results suggest that the facile H_2S adsorption/desorption and high recovery rate of the Fe-CuO sensors can be attributed to the multivalency of Fe ions and their facile redox reactions. To further investigate the role of transition metal ion's redox capability in the reversible gas-sensing characteristics of the CuO-based H_2S sensor, the 4 at.% of Ti- and Nb-doped CuO hollow spheres (referred to as 4Ti- and 4Nb-CuO) were prepared via spray pyrolysis and their gas-sensing characteristics were evaluated at 175–250 °C under RH 80% (**Figure 5**; Figure S13, Supporting Information). The doping of Ti and Nb ions into the CuO lattice was confirmed by XRD peak shifting and Raman spectroscopy (Figure S13, Supporting Information). In addition, the multivalency of Ti (Ti^{4+}/Ti^{3+}) and Nb (Nb^{5+}/Nb^{4+}) ions was confirmed by XPS (Figure S13b_4,c_4, Supporting Information). Note that the addition of Ti and Nb decreased overall gas responses at all temperatures and significantly suppressed responses of interfering gases such as ethanol, especially at low temperatures (≤ 200 °C), resulting in high

Table 1. Comparison of H_2S-sensing performance of the Fe-doped CuO sensor and CuO-based sensors in the literatures under humid condition.[45–50]

Materials	Conc. [ppm]	Response [$R_g R_a^{-1}$ - 1]	Selectivity	Full recovery	Relative humidity [%]	Reference
4Fe-CuO hollow sphere	0.1	1.8	25	O	80	This work
CuO hollow sphere	0.1	4.17	3.72	X	80	This work
Cu_7S_4-CuO microflower	100	3	3.7	X	40	49
ZnO@CuO hollow nanosphere	100	1.2	8	O	70	50
CuO nanoneedle array	10	0.77	2.4	O	40	51
CuO nanoparticle	5	9.9	14.3	X	40	52
PdO loaded CuO	50	5.79	5	O	33	53
Cu_2O/CuO microsphere	1	4.38	19.9	O	30	54
CuO nanoarray	0.005	2.5	high	O	77	55
CuO nanoparticle	0.0001	0.2	high	O	60	56
CeO_2 coated Pd-Cu_xO nanowire	0.1	3.18	17.4	O	43	57
CuO nanosheet	1	3.2	>32	O	10	58
Polyaniline/CuO composite	8	0.25	3.13	O	60	59

selectivity to H_2S (Figure S14, Supporting Information). Moreover, in both sensors, the POR to H_2S was enhanced to 100% even at low temperatures (175 °C) (Figure 5a$_2$,b$_2$), whereas those of pure CuO were low (93.45% at 175 °C). These results clearly confirm that the doping of multi-valent metal cations into CuO is a general solution for achieving high selectivity toward H_2S and enhancing reversibility by the facile redox reaction of oxygen on the surface of the gas sensors.

For evaluating the gas-sensing stability, the 18 repetitive sensing transients of 4Fe-CuO and CuO sensor to 0.1 ppm H_2S at 175 °C and RH 80% were investigated, respectively. The 4Fe-CuO sensor showed stable and reversible gas-sensing characteristics, whereas the pure CuO sensor exhibited irreversible gas-sensing characteristics (**Figure 6a**). The 4Fe-CuO sensor also exhibited stable gas responses for 12 days (Figure 6b). The dynamic gas-sensing transients of the 4Fe-CuO sensor for 0.025–0.125 ppm H_2S at 175 °C exhibited stable sensing characteristics and a linear relationship between log scale of H_2S response and log scale of concentration. The detection limit of the sensor was calculated to be 23 ppb under the criterion of $R_g R_a^{-1} - 1 > 0.2$ (Figure 6c,d). The low detection limits of 4Fe-CuO sensor were further estimated to be 4.9 ppb when 3 sigma criterion was used or 13 ppb when a signal-to-noise ratio >5 was used as the sensing criterion, respectively. All the theoretical detection limits were considerably lower than H_2S concentrations to halitosis level. The response, selectivity, recovery status, and humidity levels of CuO-based gas sensors to H_2S reported in the literature are summarized (**Table 1**).[49–59] Note that, the selectivity to 0.1 ppm H_2S in this work was compared with 0.5–5 ppm of ethanol, acetone, hydrogen, or CO, respectively. Considering H_2S high selectivity and recovery kinetics, 4Fe-CuO sensor exhibited prominent performance to quantify the H_2S concentration in a high-humidity atmosphere (RH = 80%). Finally, in order to confirm that the sensor can detect breath H_2S from halitosis patients, the gas-sensing characteristics to simulated halitosis patient's breath (normal person's breath + 25–125 ppb H_2S) were investigated (Figure S15a, Supporting Information). The sensor exhibited a reversible gas sensing characteristic after being exposed to simulated halitosis patient's breath (Figure S15b, Supporting Information) and can quantify H_2S concentration closer to oral disease or halitosis level (25–125 ppb H_2S) in a selective manner (Figure S15c, Supporting Information). These result indicates that the 4Fe-CuO sensor is an outstanding and promising solution for personal monitoring of oral diseases and halitosis.

3. Conclusion

In this study, we successfully fabricated highly sensitive, selective, and reversible H_2S sensors using Fe-doped CuO hollow spheres to detect ppb levels of hydrogen sulfide (H_2S) in a highly humid atmosphere. All powders were synthesized by spray pyrolysis, enabling the uniform dispersion of Fe ions throughout the hollow spheres, which is important for gas-sensing characteristics. To be specific, 4 at.% Fe-doped CuO ([Fe]/[Fe]+[Cu] = 0.04) hollow spheres exhibited not only the most selective performance toward 0.1 ppm H_2S over interference gases (ethanol, acetone, CO, and H_2) but also perfect recovery after exposure to H_2S. Additionally, the study verified the improved sensor reversibility when multi-valent transition metal ions, such as Ti and Nb, were incorporated into CuO sensors. The enhanced recovery kinetics resulting from doping these ions into the CuO sensors demonstrated their remarkable H_2S sensing capabilities. The investigation of these sensing properties focused on the augmentation of redox reactions and the alteration of catalytic activity in the sensing materials. The sensors developed in this study, with the addition of transition metal ions via one-pot synthesis, can provide a solution for detecting exhaled H_2S in a selective, sensitive, and reversible manner.

4. Experimental Section

Preparation of Gas-Sensing Materials: Pure CuO and Fe-doped CuO hollow microspheres were prepared via ultrasonic spray pyrolysis of solutions containing copper nitrate trihydrate ($Cu(NO_3)_2 \cdot 3H_2O$, ≥ 99.0%, Sigma-Aldrich, USA), iron nitrate nonahydrate ($Fe(NO_3)_3 \cdot 9H_2O$, ≥ 98.0%,

Sigma-Aldrich, USA), and citric acid monohydrate ($C_6H_8O_7{\cdot}H_2O$, ≥ 99.0%, Sigma-Aldrich, USA) and subsequent heat treatment. The total metal ion concentration ([Fe] + [Cu]) and citric acid monohydrate were 0.1 and 0.05 M, respectively. Three spray solutions with different molar ratios of Fe and Cu ([Fe]/[Fe]+[Cu] = 0, 0.02, 0.04, and 0.08) were used to control the Fe concentration. The spray pyrolysis system consisted of six ultrasonic droplet generators (resonant frequency:1.7 MHz), a quartz tube reactor (inner diameter: 55 mm, length: 1200 mm), and a powder-collecting chamber. The droplets generated by the ultrasonic generator were transported to the collecting chamber via a carrier gas (air, flow rate = 10 L min^{-1}). The precursor of pure CuO and Fe-doped CuO spheres synthesized by spray pyrolysis at 700 °C were collected on a Teflon bag filter in the collecting chamber, which was converted into pure and Fe-doped CuO hollow microspheres by heat treatment at 450 °C for 2 h in air. The $CuFe_2O_4$ powders were also prepared via spray pyrolysis of solutions with [Cu]: [Fe] = 1:2 and subsequent heat treatment at 800 °C for 3 h in air.

The Ti- and Nb-doped CuO hollow spheres, doped at a concentration of 4 at.% were prepared via ultrasonic spray pyrolysis of solutions containing titanium (IV) bis(ammonium lactato) dihydroxide solution ($((CH_3CH(O\text{-})CO_2NH_4]_2Ti(OH)_2$, 50 wt% in H_2O, Sigma-Aldrich, USA), ammonium niobate (V) oxalate hydrate ($C_4H_4NNbO_9{\cdot}xH_2O$, 99.99%, Sigma-Aldrich, USA) with copper nitrate trihydrate ($Cu(NO_3)_2{\cdot}3H_2O$, ≥ 99.0%, Sigma-Aldrich, U.S.A), and citric acid monohydrate ($C_6H_8O_7{\cdot}H_2O$, ≥ 99.0%, Sigma-Aldrich, USA) and subsequent heat treatment at 450 °C for 2 h in air, referred as 4Ti- or 4Nb-CuO, respectively. The experimental details regarding the simulated breath measurement system, sensor measurement system (Figures S15 and S16, Supporting Information), and characterization are provided in the Supporting Information.

Supporting Information

Supporting Information is available from the Wiley Online Library or from the author.

Acknowledgements

K.B.K. and M.S.S. contributed equally to this work. This research was supported by the National Research Foundation of Korea (NRF) grant funded by the Korea government (MSIT; No. 2021M3H4A3A02086430). This research was supported by the MOTIE (Ministry of Trade, Industry, and Energy) in Korea, under Human Resource Development Program for Industrial Innovation (Global) (P0017311) supervised by the Korea Institute for Advancement of Technology (KIAT).

Conflict of Interest

The authors declare no conflict of interest.

Data Availability Statement

The data that support the findings of this study are available from the corresponding author upon reasonable request.

Keywords

breath hydrogen sulfide, gas sensors, halitosis, oxide semiconductor, redox reaction

Received: October 7, 2023
Revised: January 19, 2024
Published online:

[1] W. Cao, Y. Duan, *Clin. Chem.* **2006**, *52*, 800.
[2] J. Pereira, P. Porto-Figueira, C. Cavaco, K. Taunk, S. Rapole, R. Dhakne, H. Nagarajaram, J. S. Câmara, *Metabolites* **2015**, *5*, 3.
[3] S. Das, M. Pal, *J. Electrochem. Soc.* **2020**, *167*, 037562.
[4] T. L. Mathew, P. Pownraj, S. Abdulla, B. Pullithadathil, *Diagnostics* **2015**, *5*, 27.
[5] C. Lourenço, C. Turner, *Metabolites* **2014**, *4*, 465.
[6] A. M. W. T. van den Broek, L. Feenstra, C. de Baat, *J. Dent.* **2007**, *35*, 627.
[7] A. Tangerman, E. G. Winkel, *J. Breath Res.* **2010**, *4*, 017003.
[8] Y. Suzuki, J. Saito, M. Munakata, Y. Shibata, *Allergol. Int.* **2021**, *70*, 181.
[9] J. Zhang, X. Wang, Y. Chen, W. Yao, *Respirology* **2014**, *19*, 1165.
[10] P. Wang, G. Zhang, T. Wondimu, B. Ross, R. Wang, *Exp. Physiol.* **2011**, *96*, 847.
[11] G. D. Banik, A. De, S. Som, S. Jana, S. B. Daschakraborty, S. Chaudhuri, M. Pradhan, *J. Breath Res.* **2016**, *10*, 026010.
[12] N. Yamazoe, G. Sakai, K. Shimanoe, *Catal. Surv. Asia* **2003**, *7*, 63.
[13] S.-Y. Jeong, J.-S. Kim, J.-H. Lee, *Adv. Mater.* **2020**, *32*, 2002075.
[14] Y. K. Moon, K. B. Kim, S.-Y. Jeong, J.-H. Lee, *Chem. Commun.* **2022**, *58*, 5439.
[15] K. B. Kim, Y. K. Moon, T.-H. Kim, B.-H. Yu, H.-Y. Li, Y. C. Kang, J.-W. Yoon, *Sens. Actuator B-Chem.* **2023**, *386*, 133750.
[16] S. H. Kim, Y. K. Moon, J.-H. Lee, Y. C. Kang, S.-Y. Jeong, *J. Mater. Chem. A* **2023**, *11*, 1159.
[17] Y. K. Moon, J.-H. Kim, S.-Y. Jeong, S. M. Lee, S. J. Park, T. H. Kim, J.-H. Lee, Y. C. Kang, *J. Mater. Chem. A* **2023**, *11*, 666.
[18] Y. K. Moon, S.-Y. Jeong, Y.-M. Jo, Y. K. Jo, Y. C. Kang, J.-H. Lee, *Adv. Sci.* **2021**, *8*, 2004078.
[19] H. Kim, C. Jin, S. Park, S. Kim, C. Lee, *Sens. Actuator B-Chem.* **2011**, *161*, 594.
[20] F. Zhang, A. Zhu, Y. Luo, Y. Tian, J. Yang, Y. Qin, *J. Phys. Chem. C* **2010**, *144*, 19214.
[21] S. Sonia, P. Suresh Kumar, N. D. Jayram, Y. Masuda, D. Mangalaraj, C. Lee, *RSC Adv.* **2016**, *6*, 24290.
[22] J. Chen, K. Wang, L. Hartman, W. Zhou, *J. Phys. Chem. C* **2008**, *112*, 16017.
[23] L. Urfels, P. Gélin, M. Primet, E. Tena, *Top. Catal.* **2004**, *30*, 427.
[24] J. D. Prades, A. Cirera, J. R. Morante, *J. Electrochem. Soc.* **2007**, *154*, H675.
[25] M. Ahmadian, M. Anbia, M. Rezaie, *Ind. Eng. Chem. Res.* **2020**, *59*, 21642.
[26] M. Iwamoto, Y. Yoda, N. Yamazoe, T. Seiyama, *J. Phys. Chem.* **1978**, *82*, 2564.
[27] Y. Gao, N. Zhang, C. Wang, F. Zhao, Y. Yu, *ACS Appl. Energ. Mater.* **2020**, *3*, 666.
[28] P. S. Murthy, V. Venugopalan, D. D. Arunya, S. Dhara, R. Pandiyan, A. I. Tyagi, *Int. Conf. on Nanoscience, Engineering and Technology (ICONSET 2011)*, IEEE, New Jersey, USA **2011**.
[29] A. Chauhan, R. Verma, K. M. Batoo, S. Kumari, R. Kalia, R. Kumar, M. Hadi, E. H. Raslan, A. Imran, *J. Mater. Res.* **2021**, *36*, 1496.
[30] R. S. Yadav, J. Havlica, J. Masilko, L. Kalina, J. Wasserbauer, M. Hajdúchová, V. Enev, I. Kuřitka, Z. Kožáková, *J. Supercond. Nov. Magn* **2016**, *29*, 759.
[31] M. Chaudhary, M. Singh, A. Kumar, Prachi, Y. K. G., A. K. Malik, Y. Kumar, B. P. Singh, *Ceram. Int.* **2021**, *47*, 2094.
[32] S. Manna, S. K. De, *J. Magn. Magn. Mater.* **2010**, *322*, 2749.
[33] A. A. Oliveira, M. I. Valerio-Cuadros, L. F. S. Tupan, F. F. Ivashita, A. Paesano, *Mater. Lett.* **2018**, *229*, 327.
[34] H. Naatz, S. Lin, R. Li, W. Jiang, Z. Ji, C. H. Chang, J. Koser, J. Thoming, T. Xia, A. Nel, L. Madler, S. Pokhrel, *ACS Nano* **2017**, *11*, 501.
[35] A. S. Adeleye, S. Pokhrel, L. Mädler, A. A. Keller, *Water Res.* **2018**, *132*, 12.

[36] K. Musa-Veloso, S. S. Likhodii, S. C. Cunnane, *Am. J. Clin. Nutr.* **2002**, *76*, 65.
[37] P. Španěl, D. Smith, *Mass Spectrom. Rev.* **2015**, *30*, 236.
[38] I. Horvath, S. Loukides, T. Wodehouse, S. A. Kharitonov, P. J. Cole, P. J. Barnes, *Thorax* **1998**, *53*, 867.
[39] J. F. Yang, M. Fox, H. Chu, X. Zheng, Y. Q. Long, D. Pohl, M. Fried, N. Dai, *World J. Gastroenterol.* **2015**, *21*, 7563.
[40] N. S. Ramgir, S. K. Ganapathi, M. Kaur, N. Datta, K. P. Muthe, D. K. Aswal, S. K. Gupta, J. V. Yakhmi, *Sens. Actuator B-Chem.* **2010**, *151*, 90.
[41] D. A. Svintsitskiy, T. Y. Kardash, O. A. Stonkus, E. M. Slavinskaya, A. I. Stadnichenko, S. V. Koscheev, A. P. Chupakhin, A. I. Boronin, *J. Phys. Chem. C* **2013**, *117*, 14588.
[42] L. Ma, D. Han, H. Ma, L. Liu, H. Guo, *Catalysts* **2018**, *8*, 635.
[43] Z. Xiao, S. Jin, X. Wang, W. Li, J. Wang, C. Liang, *J. Mater. Chem.* **2012**, *22*, 16598.
[44] N. Ma, K. Suematsu, M. Yuasa, K. Shimanoe, *ACS Appl. Mater. Interfaces* **2015**, *7*, 15618.
[45] K. Suematsu, K. Watanabe, A. Tou, Y. Sun, K. Shimanoe, *Anal. Chem.* **2018**, *90*, 1959.
[46] J.-S. Kim, K. B. Kim, H.-Y. Li, C. W. Na, K. Lim, Y.-K. Moon, J.-W. Yoon, J.-H. Lee, *J. Mater. Chem. A* **2021**, *9*, 16359.
[47] G. Litt, C. Almquist, *Appl. Catal. B-Environ.* **2009**, *90*, 10.
[48] C. Hu, C. Zhou, H. Zhang, Y. Yan, *New J. Chem.* **2023**, *47*, 11051.
[49] N. Wang, R. Jin, Y. Zhou, L. Zhao, T. Wang, L. Zhao, F. Liu, X. Yan, C. Wang, P. Sun, G. Lu, *Sens. Actuator B-Chem.* **2022**, *350*, 130847.
[50] Y. Tang, Y. Huang, H. Y. Zou, L. Wu, Z. L. Xiao, J. L. Zeng, L. X. Sun, D. Yu, Z. Cao, *Anal. Methods* **2022**, *14*, 2866.
[51] Q. Hu, W. Zhang, X. Wang, Q. Wang, B. Huang, Y. Li, X. Hua, G. Liu, B. Li, J. Zhou, E. Xie, Z. Zhang, *Sens. Actuator B-Chem.* **2021**, *326*, 128993.
[52] F. Peng, Y. Sun, Y. Lu, W. Yu, M. Ge, J. Shi, R. Cong, J. Hao, N. Dai, *Nanomaterials* **2020**, *10*, 774.
[53] M. Dun, M. Tang, D. Zhao, X. Li, X. Huang, *Sens. Actuator B-Chem.* **2022**, *358*, 131520.
[54] F. N. Meng, X. P. Di, H. W. Dong, Y. Zhang, C. L. Zhu, C. Li, Y. J. Chen, *Sens. Actuator B-Chem.* **2013**, *182*, 197.
[55] Z. Huang, X. Wang, F. Sun, C. Fan, Y. Sun, F. Jia, G. Yin, T. Zhou, B. O. Liu, *Mater. Des.* **2021**, *201*, 109507.
[56] D. Li, Y. Tang, D. Ao, X. Xiang, S. Wang, X. Zu, *Int. J. Hydrog. Energy* **2019**, *44*, 3985.
[57] W. H. Tan, X. H. Li, F. Y. Xu, D. C. Wang, J. Q. Geng, C. Zhang, J. H. Hu, X. T. Huang, B. W. Zhang, X. J. Chen, *Sens. Actuator B-Chem.* **2023**, *376*, 133040.
[58] F. Zhang, A. Zhu, Y. Luo, Y. Tian, J. Yang, Y. Qin, *J. Phys. Chem. C* **2010**, *114*, 19214.
[59] B. Zhang, F. Shang, X. Shi, R. Yao, F. Wei, X. Hou, W. Li, J. Zhang, *ACS Appl. Nano Mater.* **2023**, *6*, 18413.

NANO · MICRO small

Supporting Information

for *Small*, DOI 10.1002/smll.202308963

Highly Selective and Reversible Detection of Simulated Breath Hydrogen Sulfide Using Fe-Doped CuO Hollow Spheres: Enhanced Surface Redox Reaction by Multi-Valent Catalysts

Ki Beom Kim, Myung Sung Sohn, Sunhong Min, Ji-Wook Yoon, Jin-Sung Park, Ju Li, Young Kook Moon and Yun Chan Kang**

((Supporting Information can be included here using this template))

Supporting Information

Highly Selective and Reversible Detection of Simulated Breath Hydrogen Sulfide using Fe-doped CuO Hollow Spheres: Enhanced Surface Redox Reaction by multi-valent Catalysts

Ki Beom Kim, Myung Sung Sohn, Sunhong Min, Ji-Wook Yoon, Jin-Sung Park, Ju Li, Young Kook Moon, and Yun Chan Kang**

K. B. Kim, M. S. Sohn, S. Min, J.-S. Park, Y. C. Kang
Department of Materials Science and Engineering
Korea University
Seoul 02841, Republic of Korea
E-mail: yckang@korea.ac.kr

J.-W. Yoon
Department of Information Materials Engineering, Division of Advanced Materials Engineering
Jeonbuk National University
Jeonju 54896, Republic of Korea

J.-S. Park, J. Li
Department of Nuclear Science and Engineering,
Massachusetts Institute of Technology,
Cambridge, MA, USA

J. Li
Department of Materials Science and Engineering,
Massachusetts Institute of Technology,
Cambridge, MA, USA

Y. K. Moon
Department of Functional Ceramics, Ceramic Materials Division
Korea Institute of Materials Science (KIMS)
Changwon 51508, Republic of Korea
E-mail: ykmoon@kims.re.kr

Keywords: gas sensors, breath hydrogen sulfide, redox reaction

Experimental Section

Supplementary Fabrication of gas sensors and measuring gas sensing characteristics

Pure CuO and Fe-doped CuO powders (0.015 g) were mixed with binder (FCM, a terpineol-based ink vehicle, USA) (0.060 g) to make slurry. The gas sensing films were prepared by screen printing process on the alumina substrate (size: 1.5 x 1.5 mm^2) where two Au electrode (electrode gap: 200 µm) on the top surface and a micro-heater on the bottom surface. Power consumption of the micro-heater was 134–218 mW in the range of operating temperature (175–250 ℃). Then, to remove organic binder, they were heat-treated in box furnace at 400 ℃ for 2h. Before gas measurements, to stabilize sensors at gas sensing temperatures (175–250 ℃), the sensors were heat treated by micro-heater at 350 ℃ for 2h. After stabilization, sensors were placed in a specially designed quartz tube (inner volume: 1.5 cm^3) for investigating the gas sensing characteristics (Figure S16). Gas flow fixed constantly (200 cm^3 min^{-1}) and gas atmosphere were converted by an automatic 4-way valve from air to analyte gas and vice-versa. The relative humidity (RH) of the gas (gas temperature: 25 °C) was fixed at 80% and the gas concentrations were controlled by mixing the gases (5 ppm H_2S, acetone, ethanol, carbon monoxide, and 100 ppm hydrogen, ammonia in an air balance) with dried or humidified synthetic air. Two-prove DC resistance of the sensors was measured using an electrometer (6487 picoammeter/voltage source, Keithley, USA) connected to a computer. Gas concentration for each analyte gases were hydrogen sulfide (0.1 ppm), acetone (0.5 ppm), ethanol (1 ppm), carbon monoxide (5 ppm), ammonia (5 ppm), and hydrogen (20 ppm) and they were measure at 175–250 ℃.

Supplementary Material characterization

Field-emission scanning electron microscopy (FE-SEM; TESCAN, VEGA3) and high-resolution transmission electron microscopy with an accelerating voltage of 200 kV (HR-TEM, JEM-2100F, JEOL) were used to investigate the morphologies and microstructures of the gas sensing materials. Pore-size distributions and specific surface areas (SSAs) of sensing materials were investigated by Brunauer–Emmett–Teller (BET) nitrogen adsorption/desorption measurements (TriStar 3000, Micrometrics Instrument Co., USA). The phases and crystal structures of sensing materials were studied using X-ray diffraction (XRD, SmartLab, Rigaku Co., Japan) using Cu Kα radiation (λ = 1.5412 Å) and a Raman spectrometer (LabRam ARAMIS IR2, Horiba Jobin Yvon Co., France). The chemical states of sensing materials were investigated using X-ray photoelectron spectroscopy (XPS) (ESCALAB-250 with Al Kα radiation).

The enhanced surface redox reaction was confirmed by Temperature-Programed Reduction by hydrogen (H_2-TPR) analysis. H_2-TPR analysis of CuO and Fe-doped CuO were performed in a quartz tube micro-reactor connected to an Auto Chem 2920 instrument. Before the test, ~40 mg of sample was loaded into an U-type quartz reactor and pretreated under He flow (50 cc min^{-1}) at 350 °C for 1 h. After being cooled down to room temperature, the sample was exposed to a 10 % H_2/Ar (50 cc min^{-1}) and heated to 500 °C at a rate of 5 °C min^{-1}. The effluent was analyzed with a thermal conductive detector (TCD).

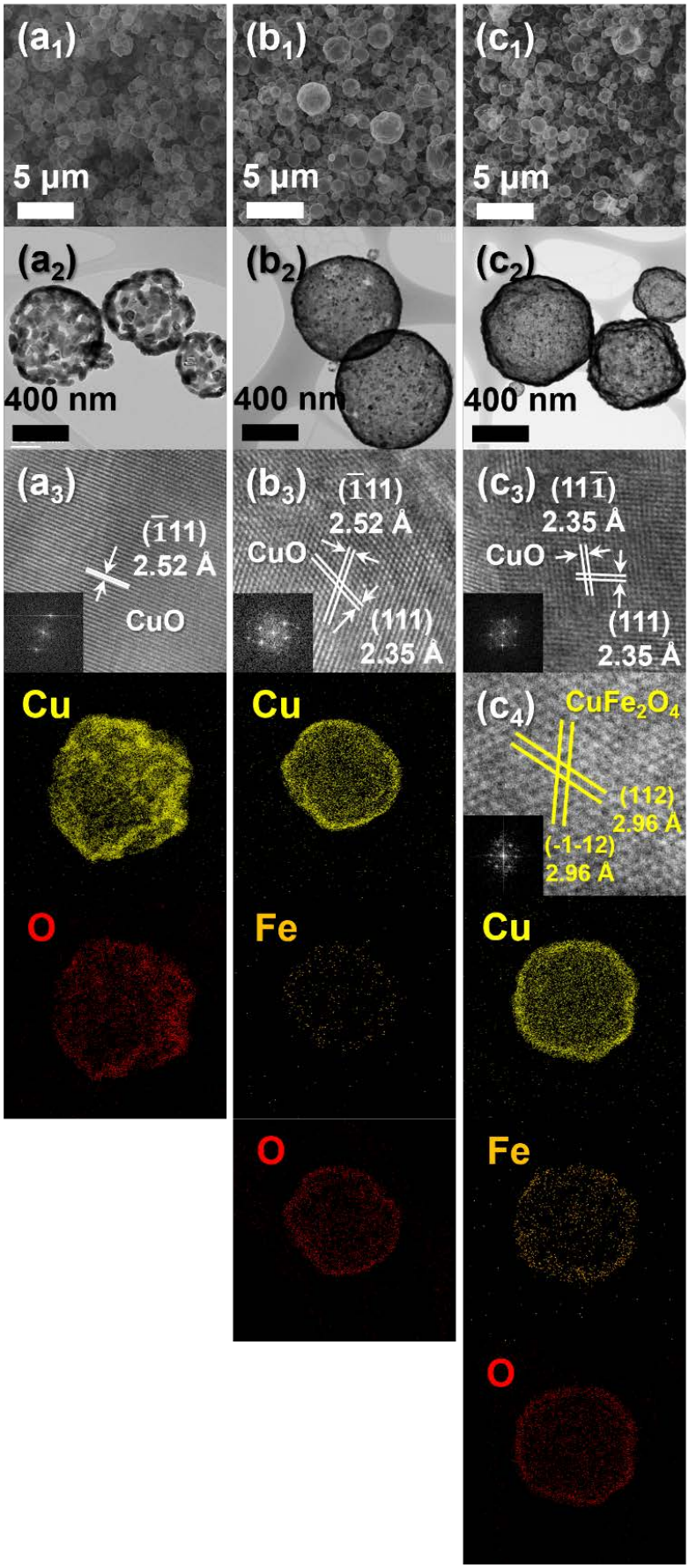

Figure S1. SEM, TEM, lattice fringes, and elemental mapping images of (a_1-a_3) pure, (b_1-b_3) 2Fe-, and (c_1-c_4) 8Fe-CuO hollow spheres.

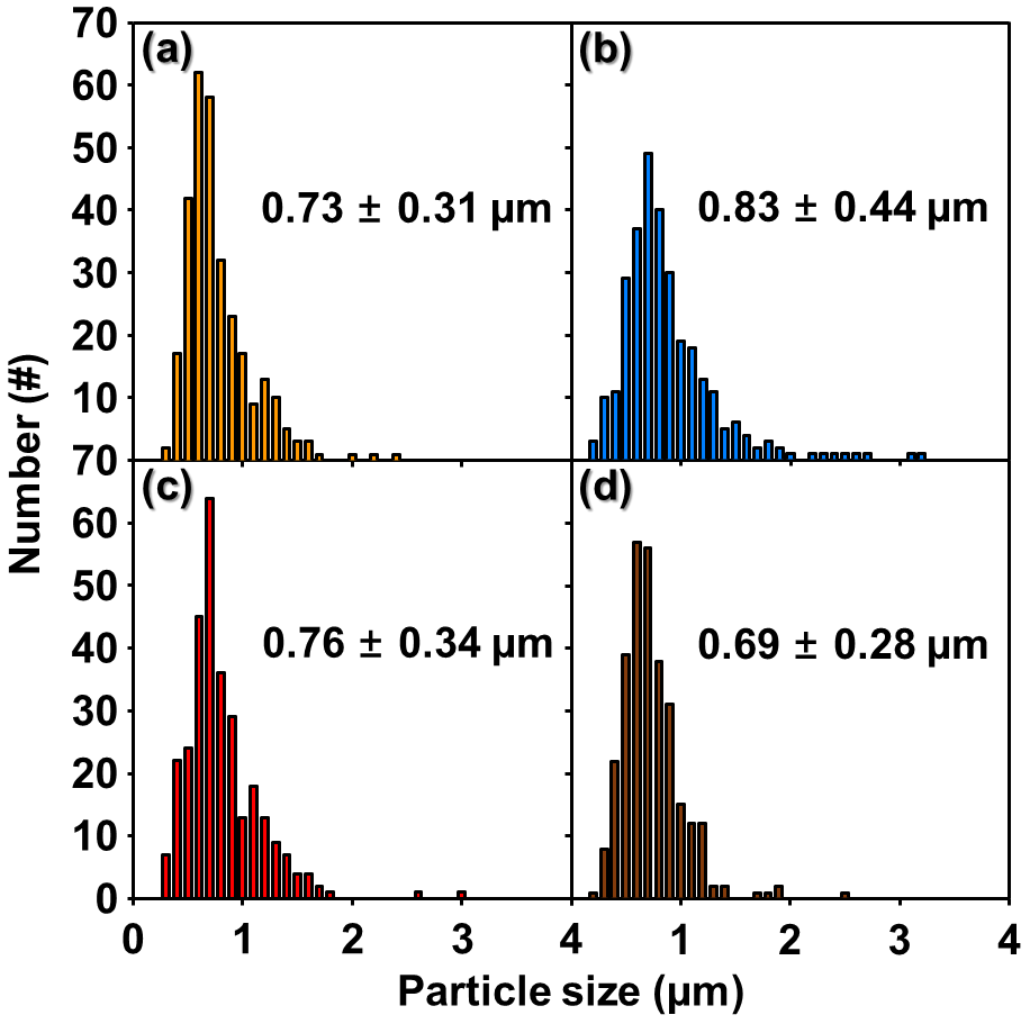

Figure S2. Particle size distributions of (a) pure, (b) 2Fe-, (c) 4Fe-, and (d) 8Fe-CuO hollow spheres.

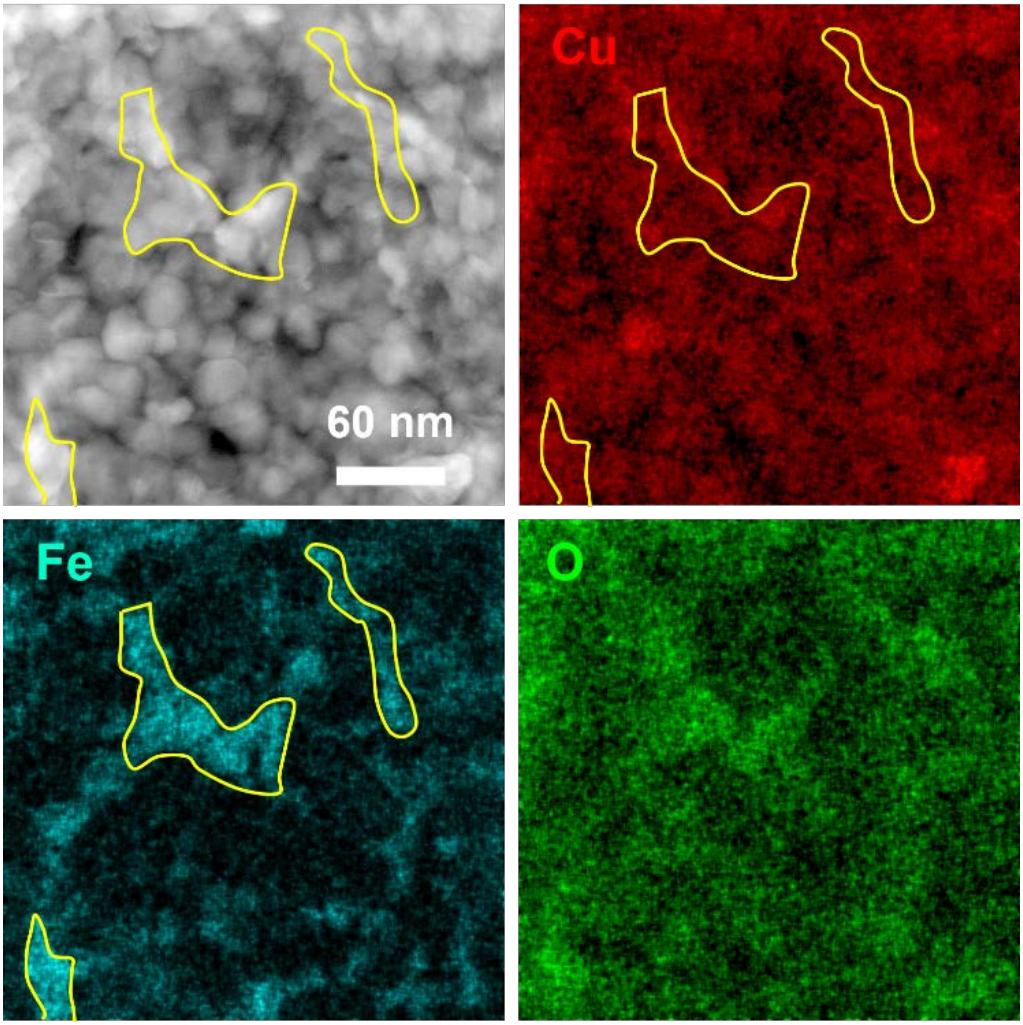

Figure S3. TEM elemental mapping images of 8Fe-CuO hollow spheres.

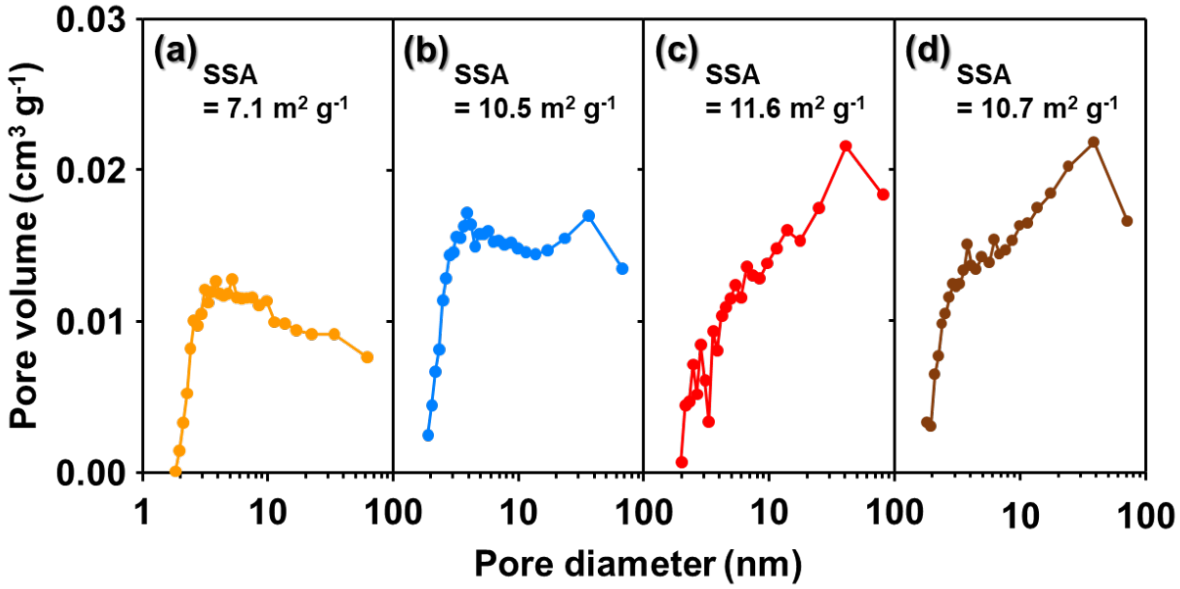

Figure S4. Pore size distributions and SSAs of (a) pure, (b) 2Fe-, (c) 4Fe-, and (d) 8Fe-CuO.

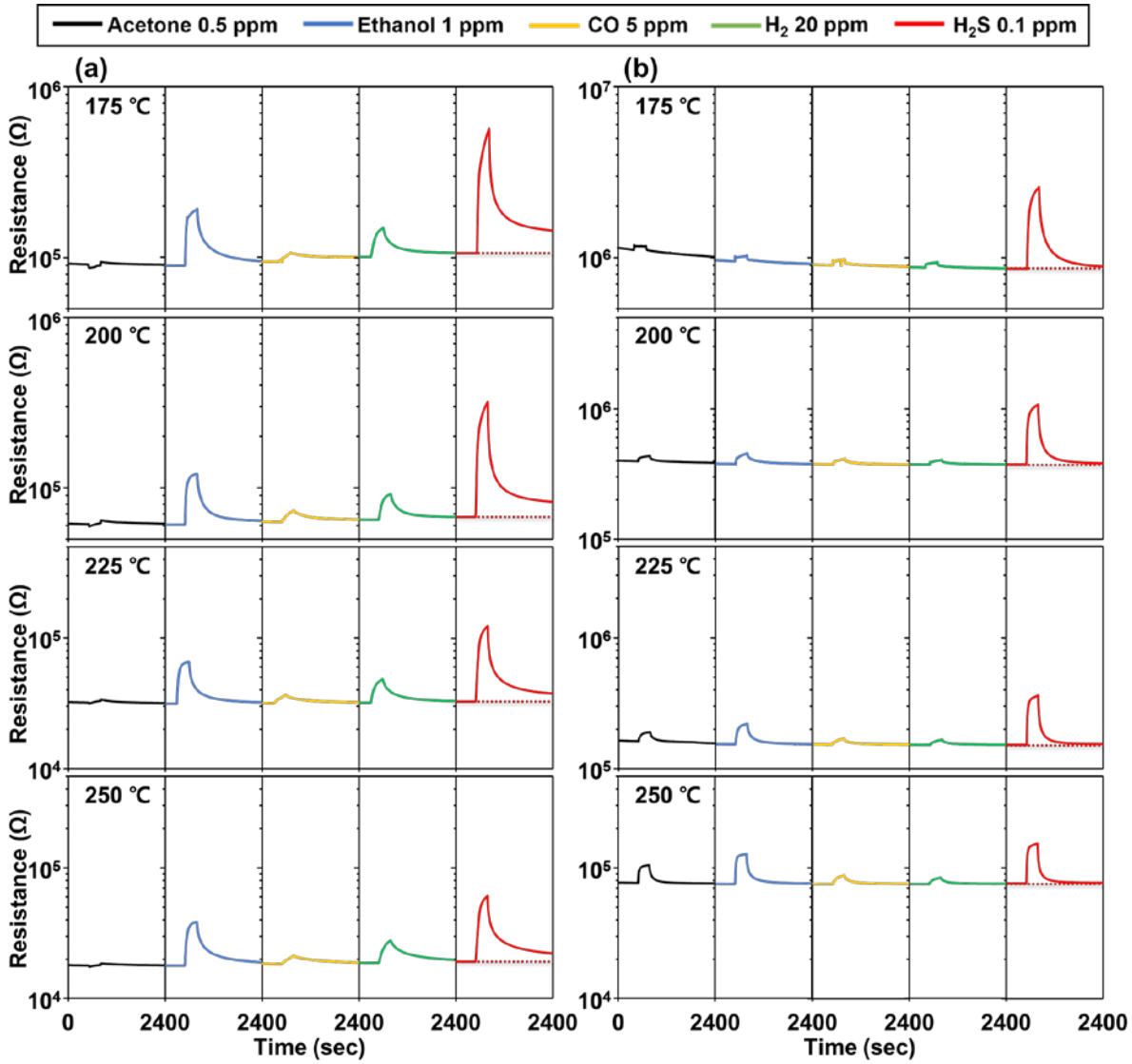

Figure S5. Dynamic sensing transients of (a) pure CuO and (b) 4Fe-CuO sensors to analyte gases under RH 80% atmosphere.

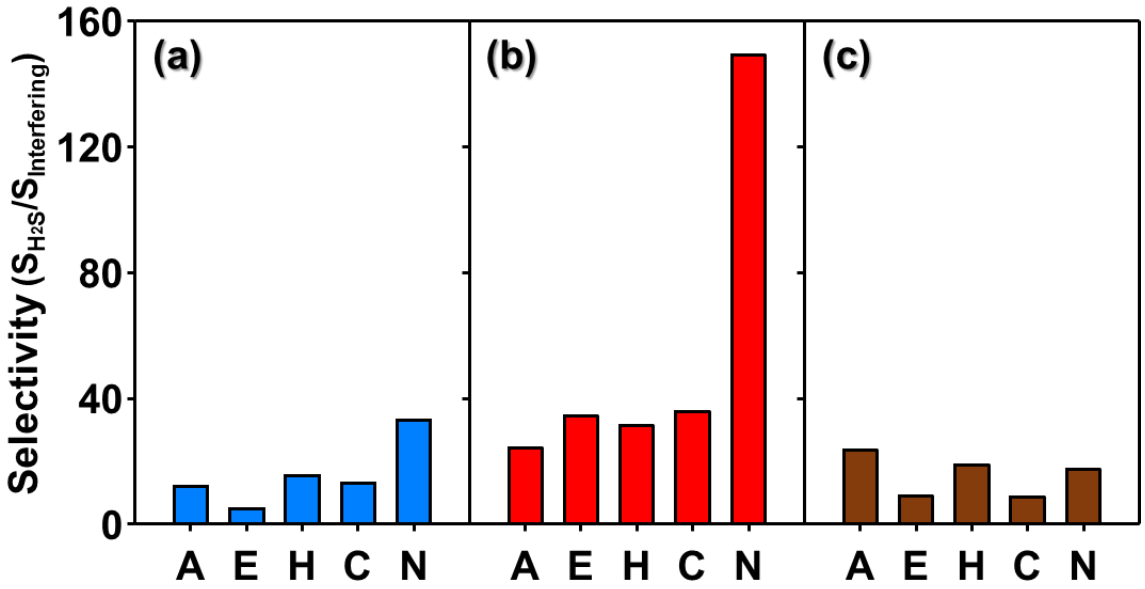

Figure S6. The selectivity values of (a) 2Fe-, (b) 4Fe-, and (c) 8Fe-CuO to 0.1 ppm H_2S at 175 ℃ (A: Acetone, E: Ethanol, H: Hydrogen, C: Carbon monoxide, N: Ammonia).

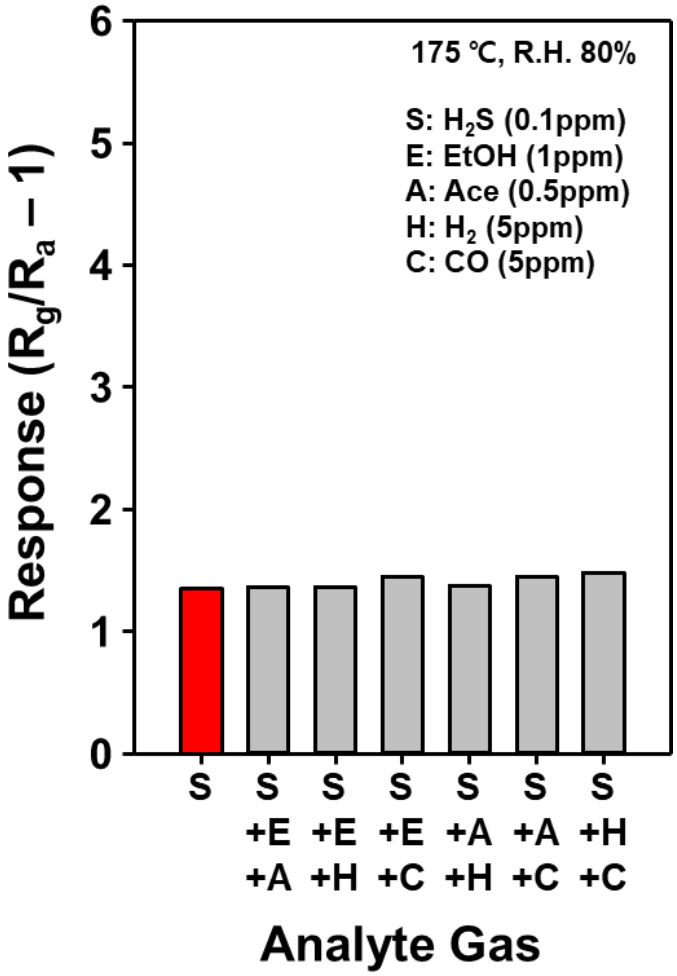

Figure S7. Gas response of 4Fe-CuO sensor to H_2S and mixed gas environment with interfering gases at 175 ℃ with RH 80%.

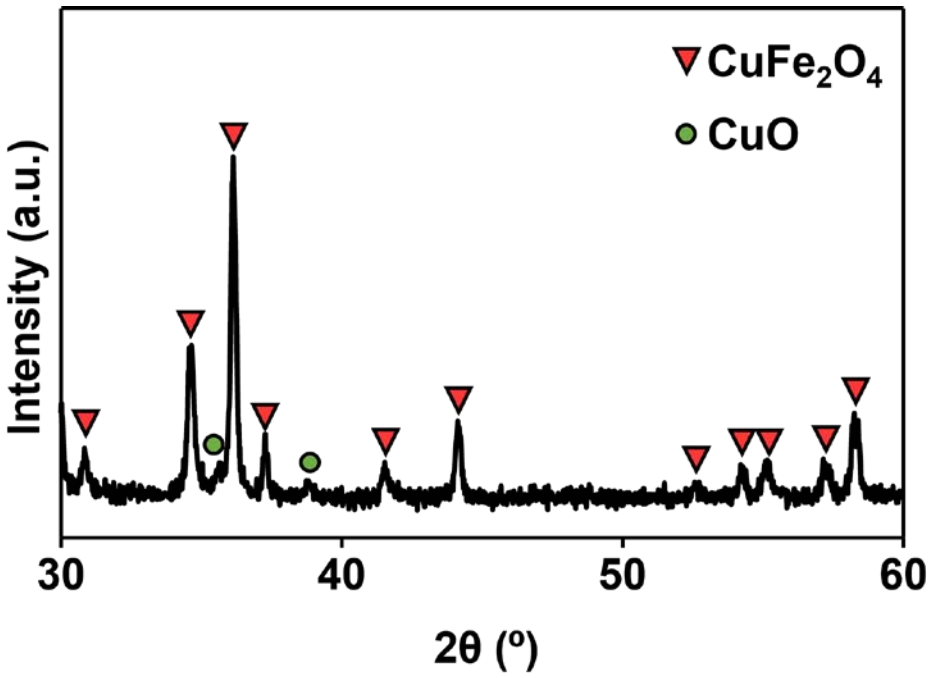

Figure S8. X-ray diffraction pattern of $CuFe_2O_4$ powders prepared by spray pyrolysis and subsequent heat treatment.

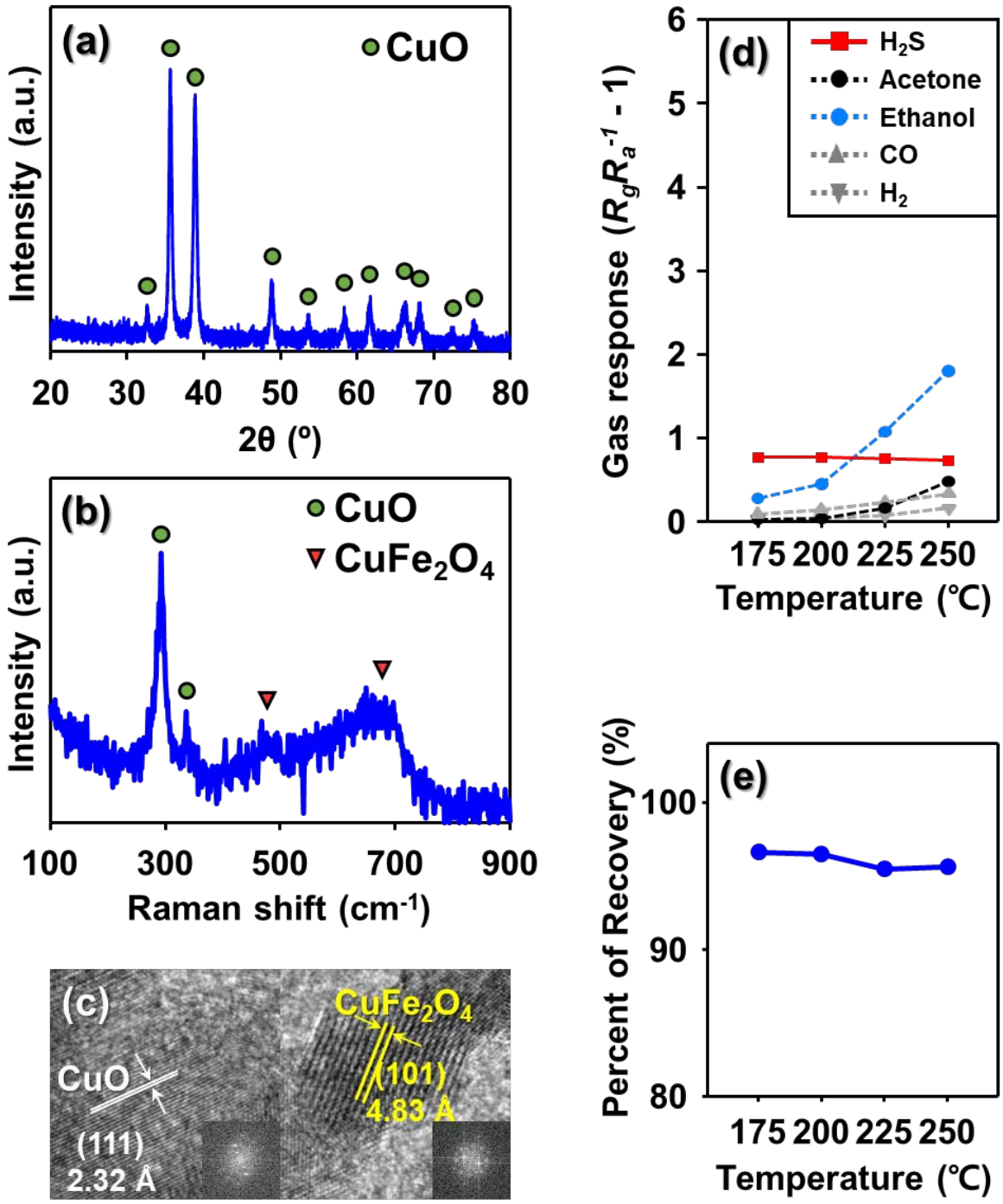

Figure S9. (a) X-ray diffraction pattern, (b) Raman spectroscopy, (c) HR-TEM images, and (d, e) gas sensing characteristics of 20Fe-CuO hollow spheres to 0.1 ppm H_2S, 0.5 ppm Acetone, 1 ppm Ethanol, 5 ppm CO, 20 ppm H_2 at 175-250 ℃ with RH 80%.

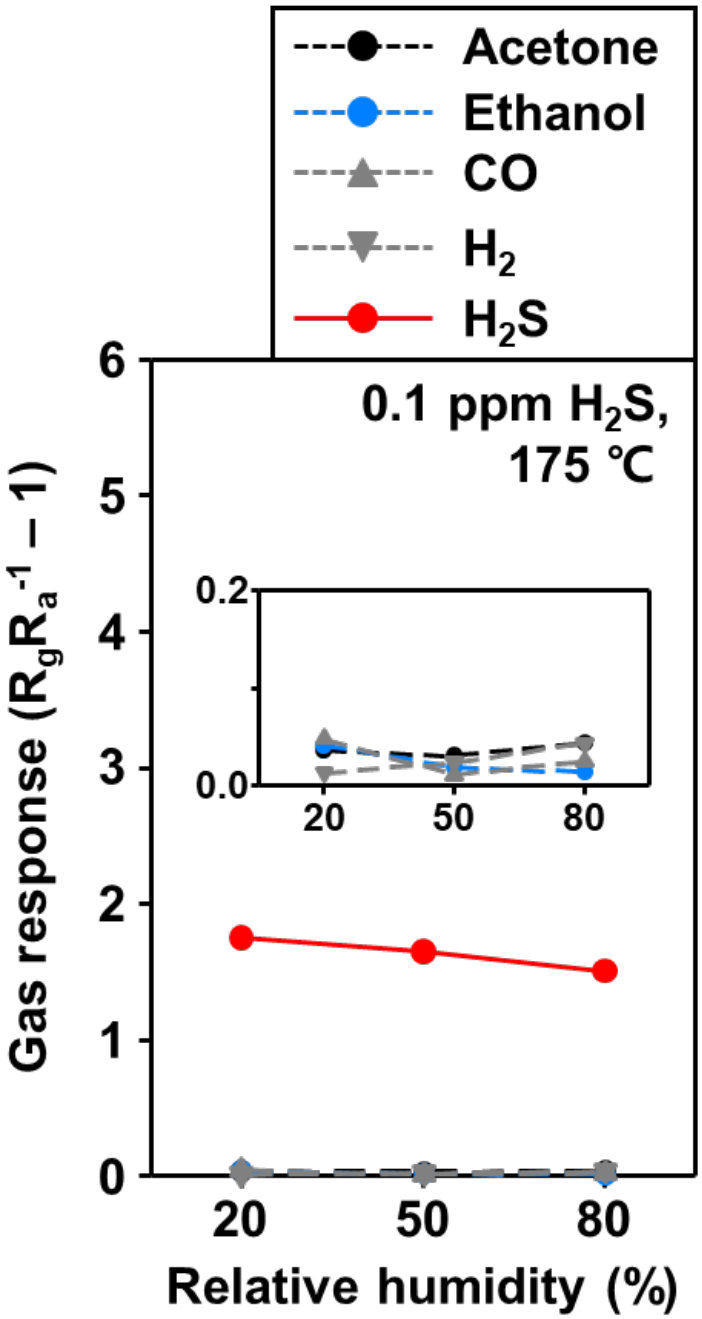

Figure S10. The gas response of 4Fe-CuO sensor to H_2S and interfering gases at 175 ℃ with various relative humidity (RH 20, 50, and 80%).

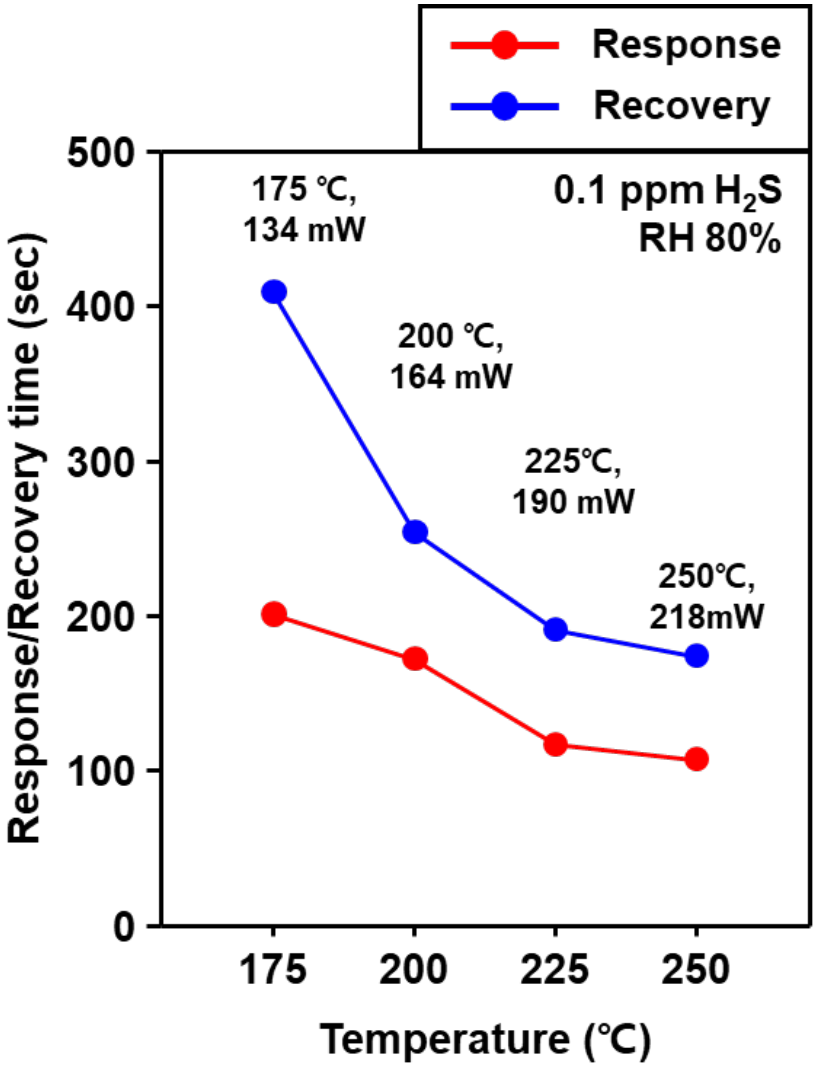

Figure S11. The response and recovery times of 4Fe-CuO sensor to 0.1 ppm H_2S at RH 80% overall the sensing temperature (125–225 °C).

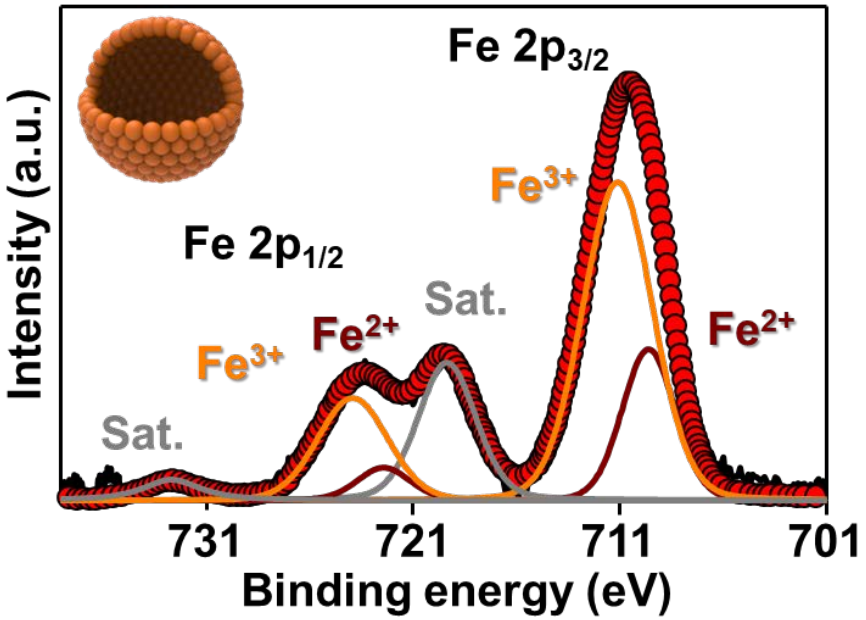

Figure S12. X-ray photoelectron spectra of Fe 2p orbital; 4Fe-CuO hollow spheres.

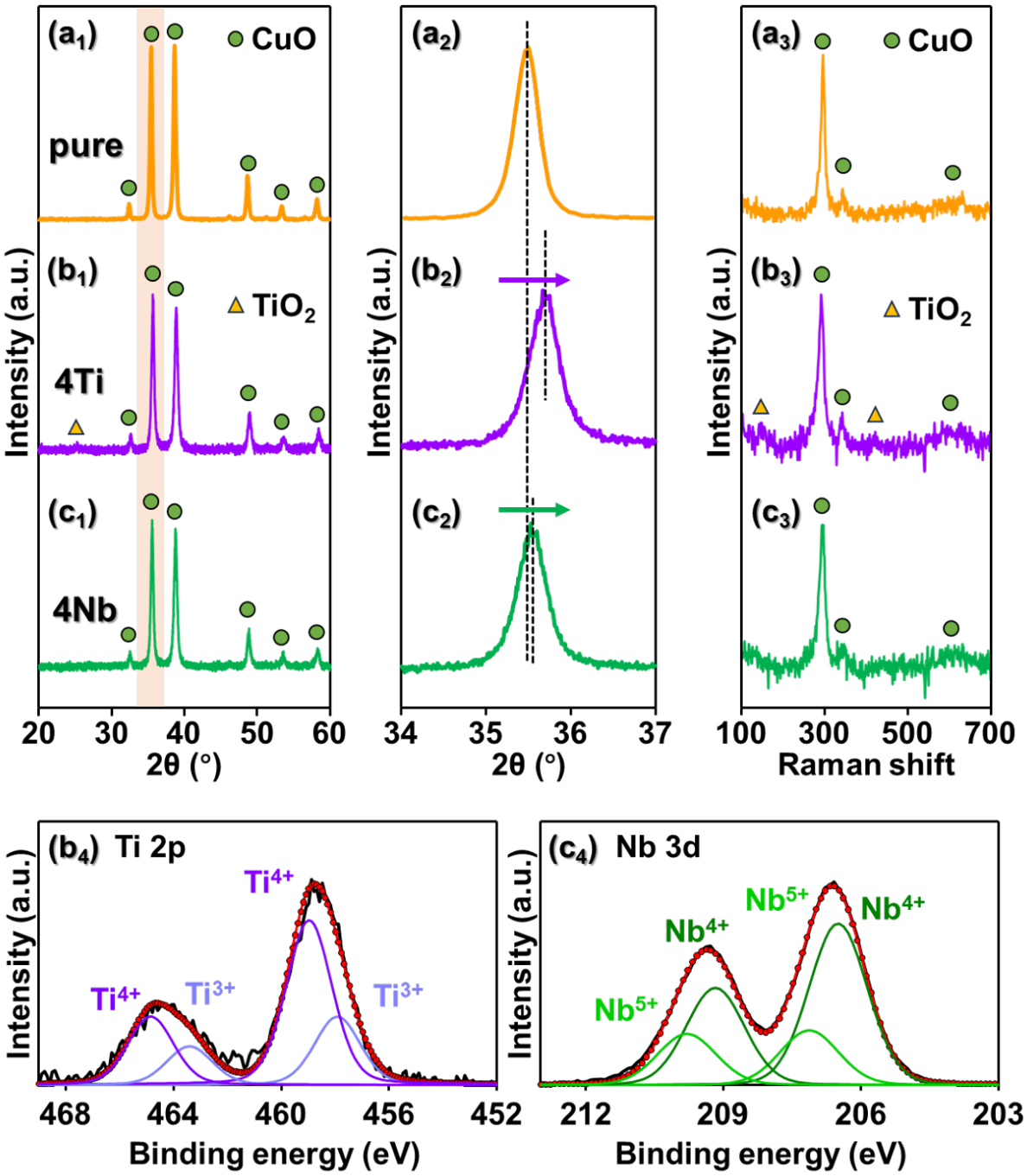

Figure S13. X-ray diffraction patterns of (a_1-a_2) pure, (b_1-b_2) 4Ti-, and (c_1-c_2) 4Nb-CuO spheres. Raman spectroscopy of (a_3) pure, (b_3) 4Ti-, and (c_3) 4Nb-CuO and X-ray photoelectron spectra of (b_4) 4Ti-, and (c_4) 4Nb-CuO spheres.

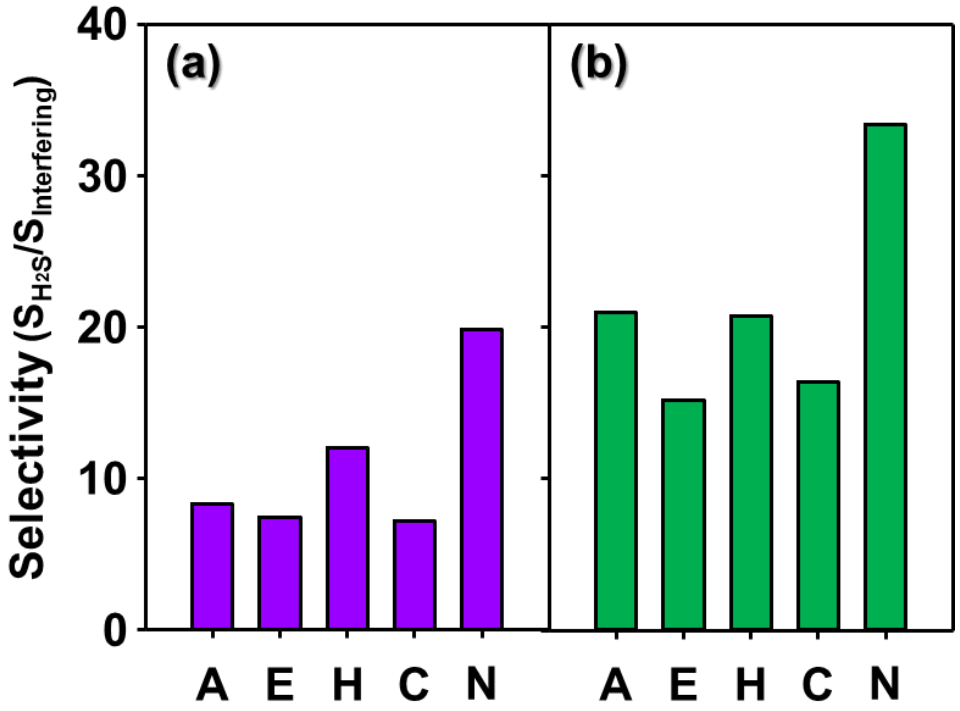

Figure S14. The selectivity values of (a) 4Ti-, and (b) 4Nb-CuO to 0.1 ppm H_2S at 175 ℃ (A: Acetone, E: Ethanol, H: Hydrogen, C: Carbon monoxide, N: Ammonia).

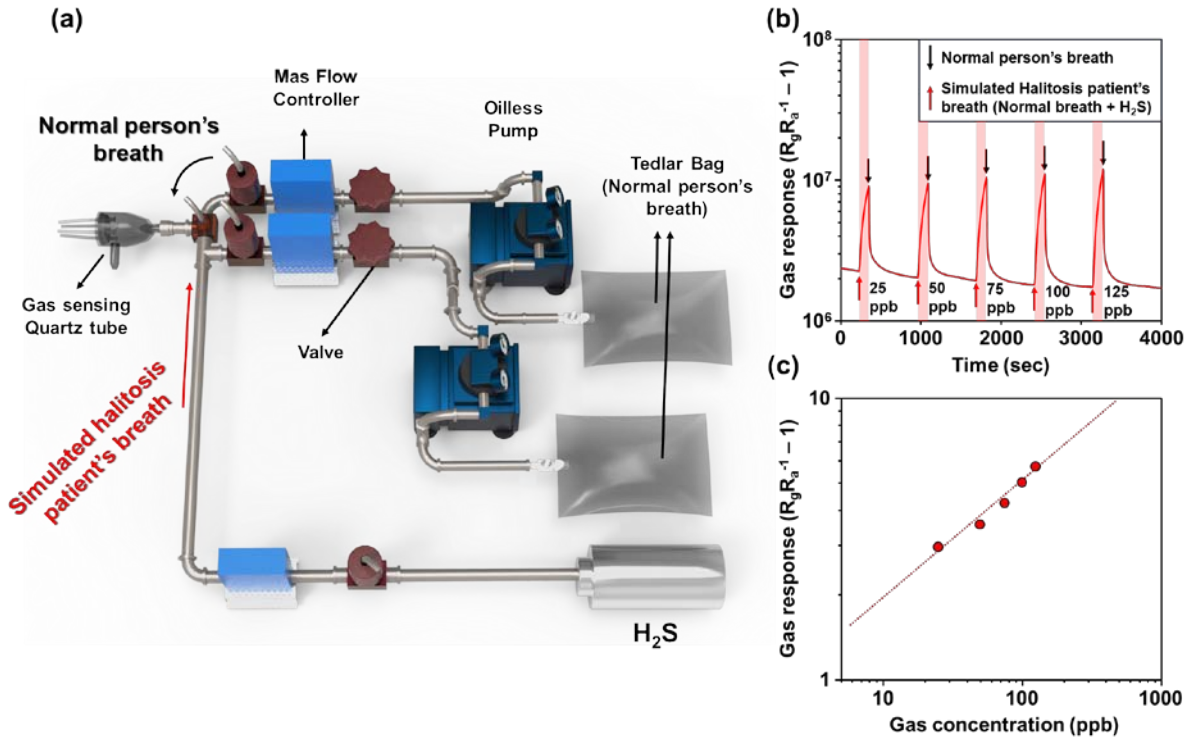

Figure S15. Schematic illustration of simulated breath measurement and gas sensing characteristics to simulated breath.

Method

The breath of normal person was collected using a 20 L Tedlar bag. The simulated breath of halitosis patient was prepared by mixing the normal person's breath and various concentrations of H_2S using the breath analysis system depicted in Figure S15a. Before sensing the simulated halitosis patient's breath, the sensor was stabilized under normal person's breath. The gas sensing characteristics of 4Fe-CuO sensor to simulated halitosis patient's breath were evaluated by changing the atmosphere from normal person's breath to halitosis patient's breath (normal person's breath + H_2S) (Figure S15b). The total flow rate was fixed at 200 sccm and the breath exposure time was 120 s.

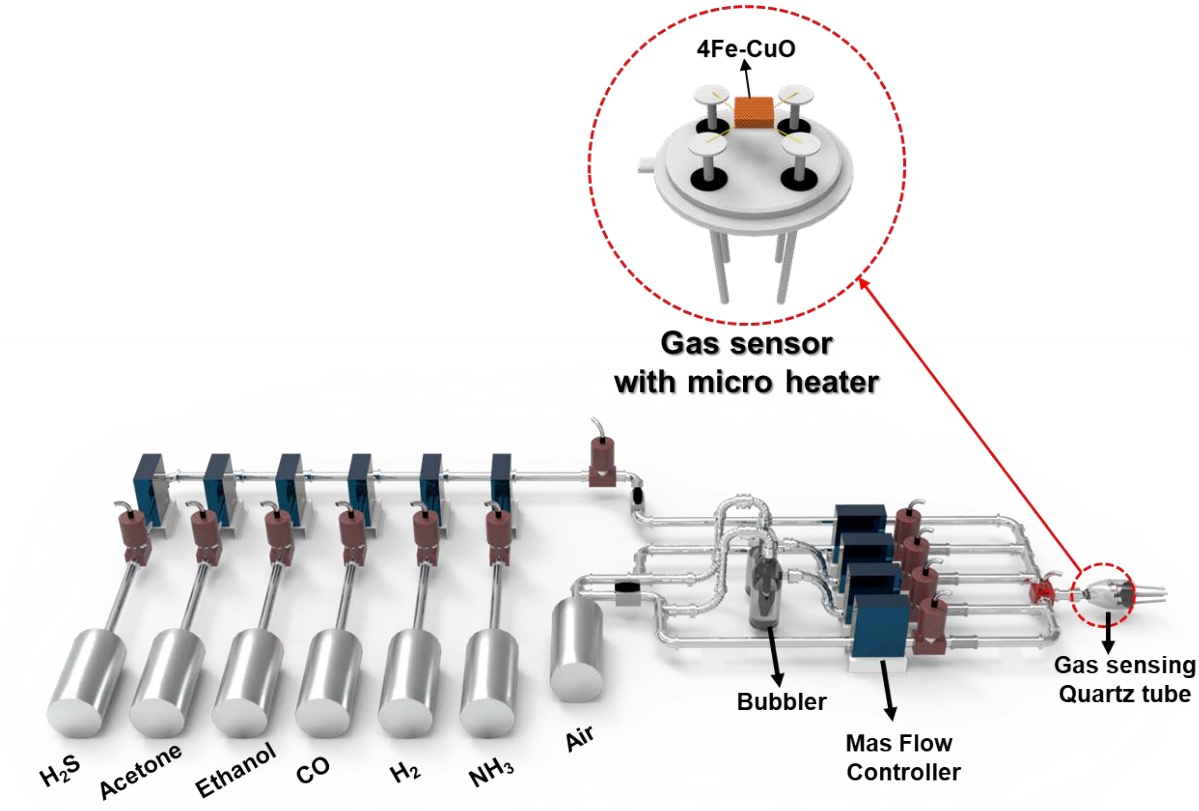

Figure S16. Schematic illustration of the gas sensor and gas sensor measurement system.